FOSSIL ENERGY

DOE/BC/15212-1
(OSTI ID: 776494)

DEVELOPMENT OF RESERVOIR CHARACTERIZATION TECHNIQUES AND PRODUCTION MODELS FOR EXPLOITING NATURALLY FRACTURED RESERVOIRS

Semi-Annual Report
July 1, 2000-December 31, 2000

By
Michael L. Wiggins
Ronald D. Evans
Raymon L. Brown
Anuj Gutpa

Date Published: March 2001

Work Performed Under Contract No. DE-AC26-99BC15212

The University of Oklahoma
Norman, Oklahoma

National Energy Technology Laboratory
National Petroleum Technology Office
U.S. DEPARTMENT OF ENERGY
Tulsa, Oklahoma

DOE/BC/15212-1
Distribution Category UC-122

Development of Reservoir Characterization Techniques and Production Models for Exploiting Naturally Fractured Reservoirs

By
Michael L. Wiggins
Ronald D. Evans
Raymon L. Brown
Anuj Gutpa

March 2001

Work Performed Under Contract DE-AC26-99BC15212

Prepared for
U.S. Department of Energy
Assistant Secretary for Fossil Energy

Thomas B. Reid, Project Manager
National Petroleum Technology Office
P.O. Box 3628
Tulsa, OK 74101

Prepared by
The University of Oklahoma
Office of Research Administration
1000 Asp Avenue, Suite 314
Norman, OK 73019

TABLE OF CONTENTS

Abstract

Development Of Reservoir Characterization Techniques And Production Models For Exploiting Naturally Fractured Reservoirs

For many years, geoscientists and engineers have undertaken research to characterize naturally fractured reservoirs. Geoscientists have focused on understanding the process of fracturing and the subsequent measurement and description of fracture characteristics. Engineers have concentrated on the fluid flow behavior in the fracture-porous media system and the development of models to predict the hydrocarbon production from these complex systems. This research attempts to integrate these two complementary views to develop a quantitative reservoir characterization methodology and flow performance model for naturally fractured reservoirs.

During the current reporting period, research has continued on characterizing and modeling the behavior of naturally fractured reservoir systems. Work has progressed on developing techniques for estimating fracture properties from seismic and well log data, developing naturally fractured wellbore models, and modifying a naturally fractured reservoir simulator. The research is currently on schedule as proposed.

One aspect of this work involved modifying popular models in terms of crack density to one that depends upon crack porosity. This modification is important because crack porosity is also used in an estimate of the permeability of a reservoir. Simple crack models are used to estimate the "dry rock" properties of a fractured reservoir. The dry rock values can then be used to predict the effects of saturation upon fractured reservoirs. For rough cracks or cracks tilted slightly from the vertical, the S-waves were found to be sensitive to the saturation. Since the S-wave splitting increase is expected for near vertical signals, S-waves show the greatest exploration potential for detecting saturation in reservoirs.

Software was developed to compute the seismic reflection coefficients. The software has been used to test some of the basic differences between a reservoir with a single fracture system and a reservoir with two fracture systems with different orientations. The results indicate that S-waves hold the key to working out some of the problems related to multiple fracture sets.

A methodology for integrating the seismic and production tests has been developed. The strength of this approach is that no scaling is involved. Here we assume that the seismic scale and the production scale are the same. The goal then is utilize the influence of the crack porosity upon both the permeability and the seismic response. A genetic algorithm and software program has been developed to obtain fracture density and aspect ratio through the inversion of fractured reservoir rock models using conventional well logs. The software is ready for further testing. Research suggests a need for logs and interwell measurements of the frequency dependent attenuation of shear and compressional sound waves.

Wellbore performance models for vertical and horizontal wells in naturally fractured reservoirs have been devoloped. These models have been incorporated into the naturally fractured reservoir simulator but have not been tested. The development of the reservoir simulator continues in a timely manner. Previous problems related to material balance errors have been corrected by modifying the numerical solution of the flow equations.

Introduction

Many existing oil and gas reservoirs in the United States are naturally fractured. It is estimated that from 70-90% of the original oil and gas in place in such complex reservoir systems are still available for recovery, provided new technology can be implemented to exploit these reservoirs in an efficient and cost effective manner. Enhanced oil recovery processes and horizontal drilling are two fundamental technologies which could be used to increase the recoverable reserves in these reservoirs by as much as 50%. This research is directed toward developing a systematic reservoir characterization methodology which can be used by the petroleum industry to implement infill drilling programs and/or enhanced oil recovery projects in naturally fractured reservoir systems in an environmentally safe and cost effective manner. It is anticipated that the results of this research program will provide geoscientists and engineers with a systematic procedure for properly characterizing a fractured reservoir system and a reservoir/horizontal wellbore simulator model which can be used to select well locations and an effective EOR process to optimize the recovery of the oil and gas reserves from such complex reservoir systems.

The focus of the research is to integrate geoscience and engineering data to develop a consistent characterization of the naturally fractured reservoir. During the current reporting period effort has focused on relating seismic data to reservoir properties of naturally fractured reservoirs, scaling well log data to generate interwell descriptors of these reservoirs, enhancing and debugging a naturally fractured reservoir simulator, and developing a horizontal wellbore model for use in the simulator.

Seismic studies can be used to compliment production tests and data regarding the development of fractured reservoirs. Fracture aperture and porosity are the key parameters in this effort and are used for constructing elastic and permeability models of fractured reservoirs tied to production. The goal of this effort is the ability to map permeability variations with the seismic. Seismic mapping of saturation is another important tool for predicting the performance of a reservoir. As it turns out, the effect of saturation upon the elastic properties of rocks depends upon the anisotropy of the dry rock. P-wave studies of saturation in fractured reservoirs require long offsets. Some types of dry rock anisotropy can make the S-waves more sensitive to saturation in fractured reservoirs than the P-waves. This opens new exploration and development possibilities using S-waves.

Seismic Amplitude Versus Offset (AVO) evaluation of fractured reservoirs requires the computation of the reflection coefficient between two arbitrary anisotropic media. Software has been developed for this purpose. Using this software a preliminary study has been made regarding AVO responses in the presence of multiple fracture systems. This study indicates that there are some techniques that can be used to find clues to the orientation of major fracture systems. The S-waves are the most indicative of these orientations. Integrating both the seismic and production data using the ideas developed in this project has lead to an improved methodology for predicting the performance of fractured reservoirs. Calibration methods using production tests have been developed to estimate important constants that can be used in mapping reservoir properties using the seismic data.

Conventional well logs may be used for fracture detection since they often exhibit abnormal values in response to fractured zones within a borehole. Efforts have focused on obtaining quantitative description and characterization of naturally fractured reservoirs using

conventional well logs. A genetic algorithm has been used to obtain fracture density and aspect ratio through the inversion of fractured reservoir rock models. The model proposed by O'Connell and Budiansky (1977, 1984) has been implemented to develop the application of genetic algorithm to this problem. The software for determination of crack density and aspect ratio from conventional well logs is ready for further testing. Research suggests a need for logs and interwell measurements of the frequency dependent attenuation of shear and compressional sound waves. Investigation further reveals that cross-well tomography measurements may offer such information. Data from multi-frequency measurements should enhance the information that can be extracted for the description of fractured reservoirs.

Development of naturally fractured wellbore models for use in the reservoir simulator is an important element of this research. After a thorough literature review, it was decided to implement a wellbore system that assumes a horizontal wellbore open to flow along its total length and with a homogenous fluid flowing through it. Flow from both the fractures and matrix is allowed to occur and is considered through productivity indexes that are proportional to the equivalent fracture and matrix permeabilities, respectively. A similar approach has been implemented for the vertical well.

Work has also progressed on developing a naturally fractured reservoir simulator for use in a PC environment. This work is ongoing and the simulator will be modified to incorporate methodologies developed in this research. Efforts have concentrated on correcting material balance problems and incorporating wellbore models within the program. One major complication with the work discussed in the last progress report was related to unacceptable material balance errors. This problem has commanded a large portion of the project time during the last six months. However, the problem has been solved and was related to the numerical solution of the mathematical model proposed by Evans (1982). Additionally, steps continue to move the program from a mainframe to a desktop computing environment. The modeling effort is proceeding in a timely fashion.

Results and Discussion

For many years, geoscientists and engineers have undertaken research to characterize naturally fractured reservoirs. Geoscientists have focused on understanding the process of fracturing and the subsequent measurement and description of fracture characteristics. Engineers have concentrated on the fluid flow behavior in the fracture-porous media system and the development of models to predict the hydrocarbon production from these complex systems. This research attempts to integrate these two complementary views to develop a quantitative reservoir characterization methodology and flow performance model for naturally fractured reservoirs.

During the current reporting period, research efforts have focused on relating seismic data to reservoir properties, determing fracture properties and interwell descriptors from well log data, developing vertical and horizontal naturally fractured wellbore models, and enhancing a naturally fractured reservoir simulator for use in making performance predictions. Details of the work conducted for the various research tasks are discussed in the following sections.

Task I. Characterize Fractured Reservoir Systems

Seismic studies offer the potential to map fractured reservoir properties. However, exploration and exploitation of fractured reservoirs is difficult because of the poorly understood relationship between the fractured reservoir properties and the seismic response. Research conducted during this reporting period address this problem.

First a variation on a conventional fracture-modeling theme was adapted to model the elastic properties of fractured reservoirs in terms of the fracture apertures. The advantage of this approach to the parameterization of fracture systems is that it ties the seismic response to the size of the fracture aperture controlling the flow through the reservoir.

Next, the effect of saturation upon reservoir properties has been investigated via the published results of Brown and Korringa (1975). This portion of the study yielded some important predictions regarding the sensitivity of shear waves to the saturation of fractured reservoirs. When the anisotropy of the dry rock breaks certain anisotropic symmetries, the shear waves can become more sensitive to the saturation than P-waves when conducting surface seismic studies. This is a very important conclusion for both development and exploration efforts.

In order to study the seismic reflection coefficient from fractured reservoirs, special software was developed to compute the reflection coefficient between two anisotropic media. This software provides the ability to model the reflection coefficient between any two anisotropic media. This software forms the foundation for the modeling and seismic interpretation involved in the project. A description of the algorithm used is given in this report.

The reflection coefficient modeling software has been used to model two basic fracture models. The simplest model consisted of a single set of fractures. The second model considered consisted of two fracture systems that are not parallel. Although the occurrence of multiple fracture systems can complicate the seismic response, there are still some seismic indicators that can be used to infer the direction of maximum permeability. This is an encouraging result when faced with the presence of multiple fracture systems.

Combining the results, a methodology has been developed for correlating the seismic response with available production data. In this way, the seismic response can, in principle, be

used to predict the production performance of wells. The remaining problem is a more complete characterization of the tie between the fracture porosity, the number of fracture systems involved and the permeability of the fracture system. At present the simplifying assumption is made that the fracture permeability is simply related to the fracture porosity via a functional relationship. Future work will expand upon this idea.

There are admittedly, many other aspects of fractured reservoirs that still need to be addressed. For example, the fluid coupling between the matrix and the fracture system is poorly quantified and completely ignored in the work accomplished thus far. In addition, the frequency-dependence of the seismic properties has not been addressed. However, the goal was to first accomplish a method of addressing the foundation of the problem. The approach chosen is not pretty and it makes many assumptions, but it can be used to give a solution. The long-term goal is to move toward the method that takes account of the frequency dependence and the coupling between the fractures and the matrix.

Relating Fracture Permeability to Seismic Response. One of the problems using conventional fracture models in practice is the inability to validate the parameters used in the model. In this section, an approach is described for relating the seismic response to the production tests within the reservoir. The section begins by examining the weakness of conventional fracture models. Then a method is developed that parameterizes the fractures in terms of fracture aperture. Fracture aperture can be directly related to the flow through the reservoir as well as the seismic response.

Popular fracture model parameters used to predict elastic properties include the aspect ratio and the fracture density. The validation of these parameters is extremely difficult even with the availability of core and modern logs. Another problem is the separate treatment of mechanical and flow properties. For example, one might suggest that the small aperture cracks control the elastic properties that are studied via seismic methods while the large aspect ratio cracks control the reservoir permeability. In reality, it is highly unlikely that the effective crack parameters controlling the elastic properties are the same as those controlling the flow. Admitting the likelihood, how do we proceed to verify both a mechanical and a flow model for the reservoir? It may be possible in a laboratory environment but it will be virtually impossible in a production environment.

One way to get around the problem of verifying fracture models is to express both the elastic model and the permeability model in terms of compatible parameters. Implicit in this approach is the assumption that the same set of cracks controls both the permeability and the elastic properties. This over-simplified approach can be expanded to account for filled cracks and un-connected cracks. Some discussion of this expansion will be given in the next section.

For the purposes of this report, the simplifying assumption is made that all of the cracks present are connected. Contrary to popular thinking, the same fracture system is assumed to control both the permeability and the elastic properties. A simple crack model for the elastic properties is described below in terms of the crack porosity. Next, the product of the crack porosity times the aperture raised to the second power is shown to control the crack permeability for a simple crack model. Combining seismic and flow measurements can be used to estimate the effective aperture and crack porosity for the reservoir.

The elastic compliance of a fractured rock can be computed using averages of strains and stresses over a selected volume (Horri and Nemat-Nasser, 1983). For example, Oda et al. (1984)

used this approach to derive an expression for the compliance of a fractured rock. The basic idea is to assume that the average or effective strain measured on the surface of a volume is due to the average strain over the matrix material that contains the fractures and the average strain over the volume of the fractures.

$$\bar{\varepsilon}_{ij} = \bar{\varepsilon}_{ij}^{M} + \bar{\varepsilon}_{ij}^{C} \qquad \text{.....1}$$

Eq. 1 can be rewritten in the following form (Horri and Nemat-Nasser, 1983).

$$\bar{\varepsilon}_{ij} = S_{ijkl}^{M}\,\bar{\sigma}_{kl} + S_{ijkl}^{C}\,\bar{\sigma}_{kl} = S_{ijkl}^{M}\,\bar{\sigma}_{kl} + \frac{1}{V_{Total}} \int_{V(Cracks)} \frac{1}{2}\left(\frac{\delta_i}{x_j} + \frac{\delta_j}{x_i}\right) dV^{C} \qquad \text{.....2}$$

where S_{ijkl} with superscript M is the compliance of the matrix without fractures and S_{ijkl} with superscript C is the excess compliance due to the presence of the fractures. These compliances are the inverse of the elastic stiffness constants typically used in geophysical exploration. The δ's in the above expression are the components of the displacement discontinuities across the cracks and the x_i's represent the distance across the crack in the i-th direction. The x_i's can be written in the following form

$$x_i = \frac{A}{n_i} \qquad \text{.....3}$$

where A is the aperture of the fracture and n_i is the i-th component (i=1,2,3) of the normal to the fracture. Writing the integral in Eq. 2 as a summation and combining with Eq. 3 yields the following relationship for the average excess strain due to the N cracks

$$\bar{\varepsilon}^{c}_{ij} = \frac{1}{V_{Total}} \sum_{m=1}^{N} \frac{1}{2}\left(\frac{\delta_i}{A_m} n_j^m + \frac{\delta_j}{A_m} n_i^m\right) \Delta V_m^{Crack} = \frac{1}{V_{Total}} \sum_{m=1}^{N} \frac{1}{2}\left(\delta_i n_j^m + \delta_j n_i^m\right) \frac{\Delta V_m^{Crack}}{A_m} \qquad \text{.....4}$$

The excess strain associated with each crack is multiplied times the volume of the crack in a weighted sum. Assuming a particular shape for the cracks can be used to assign the crack volumes in the above expression. The displacement discontinuity across a crack can be assumed to have a simple linear relationship to the traction applied to the crack.

$$\delta_i = k_1 \sigma_{ij} n_j \qquad \text{.....5}$$

The constant k_1 in Eq. 5 is related in some way to the physical properties of the crack. For example, one can assume that the constant is proportional to the diameter of the crack, D, when using penny-shaped cracks (Oda et al., 1984).

$$k_1 = k_2 D \qquad \text{.....6}$$

Substitution of Eqs. 5 and 6 into Eq. 4 yields the expression

$$\bar{\varepsilon}^{c}{}_{ij} = \frac{k_2}{V_{Total}} \sum_{m=1}^{N} \frac{1}{2} \left(\bar{\sigma}_{ik} n_k^m n_j^m + \bar{\sigma}_{jl} n_l^m n_j^m \right) \frac{D_m \Delta V_m^{Crack}}{A_m} \quad \text{.....7}$$

If the cracks all have the same orientation, the above expression simplifies to the following form.

$$\bar{\varepsilon}^{c}{}_{ij} = \frac{Z}{2} \left(\bar{\sigma}_{ik} n_k^m n_j^m + \bar{\sigma}_{jl} n_l^m n_j^m \right) = \frac{Z}{4} \left(n_j n_k \delta_{il} + n_j n_k \delta_{il} + n_j n_k \delta_{il} + n_j n_k \delta_{il} \right) \bar{\sigma}_{kl} \quad \text{.....8}$$

where Z is the specific impedance. The excess compliance due to the cracks is (modified from Schoenberg and Douma, 1998).

$$S_{ijkl}^{c} = \frac{Z}{4} \left(n_j n_k \delta_{il} + n_j n_k \delta_{il} + n_j n_k \delta_{il} + n_j n_k \delta_{il} \right) \quad \text{.....9}$$

Using the above notation, the specific impedance Z can be written in the form

$$Z = k_2 \frac{N_{Cracks} \left\langle \frac{D \Delta V^{Crack}}{A} \right\rangle}{V_{Total}} \quad \text{.....10}$$

where an average is implied inside the bracket. A crack geometry commonly used is the penny-shaped crack where the area of the crack is

$$area = \frac{\pi D^2}{4} \quad \text{.....11}$$

The volume of the crack is the area times the aperture A of the crack. The product of the number of cracks per unit volume times the average of the cubic diameter is often used in the crack literature and is given the name of fracture density (e). If we absorb the extra constants into k_2, the specific compliance for a system of aligned penny-shaped cracks can be written in the form

$$Z = k_2 e \quad \text{.....12}$$

where

$$e = N_{Cracks} \left\langle D^3 \right\rangle \quad \text{.....13}$$

Hudson (1980, 1981) uses the radius rather than the diameter in the above expression. Eq. 9 can be used to get a crack density for different crack shapes. However, the constants involved

in "crack densities" vary as the crack model and geometry varies. As a result, the term "crack density" is somewhat misused in the literature and there is no uniform definition of the term.

Another major problem with this popular parameter, crack density, is that it is difficult to directly verify or validate by any other means than the seismic response. Neither the number of cracks per unit volume or the average diameter of cracks can be readily verified with well control and/or core. Thus we are stuck with a theory that cannot easily be validated. Some other parameterization of fractures is required that can be used to tie the seismic properties to an observable quantity. Using the apertures of fractures is suggested below.

Changing the Crack Parameter Used To Model Aperture. One of the problems with current fracture models described above is that they depend upon parameters that cannot easily be obtained by any method. Fracture parameters such as aspect ratio and diameter or even the number of fractures in a unit volume are extremely difficult to verify. Aperture is not very easily obtained either. Admittedly apertures can be measured in cores and for very large apertures, certain logs might be used. However, in all of these cases, one has to wonder about the scaling issues required to accurately predict the flow at the scale of the production. There are some real problems validating any model used to describe the seismic response. However, of the fracture parameters available, the fracture aperture is the most easily visualized as having some control upon the permeability.

Now in order to focus upon the association of elastic properties with permeability, we look for ways to get the aperture into our modeling of the elastic properties. One way to accomplish this is to assume a simple linear relationship between the aperture (A) and the diameter (D) for a crack. This idea is not a new one. For example, Vermilye and Scholz (1995) studied such a relationship. Thus if the diameter is proportional to the aperture of a fracture, Eq. 6 can be written in the form

$$k_1 = k_3 A \qquad \text{.....14}$$

where k_3 absorbs the constant of proportionality between the aperture and the diameter in Eq. 6. Eq. 8 is again obtained by using Eqs. 5 and 13 with Eq. 7 with Z defined to be

$$Z = k_3 \ \phi_C \qquad \text{.....15}$$

rather than as defined in Eq. 9. The crack porosity is simply the crack pore space divided by the total volume of rock being considered. Admittedly, at this point, it is not apparent that anything has been gained by this approach. This will be more apparent when we discuss the approach to modeling the permeability. At this point the degree of fracture anisotropy is related to the crack porosity. Crack porosity then determines the strength of the anisotropy determined via seismic.

The permeability of a crack system, assuming they are all connected and can be modeled as parallel plates, can be found by summing the flow along the various fractures. For a single set of parallel fractures, the following equation can be obtained from results published by Oda (1985) or a number of petroleum engineering texts.

$$k_{ij} = \frac{A^2 \phi_C}{12}\left(\delta_{ij} - n_i n_j\right) \qquad \text{.....16}$$

Note that the crack porosity also occurs in this expression for the permeability. If the crack porosity is determined by seismic studies, then a production test and/or production data indicating the permeability k can be used to estimate the aperture (A) for the fractures involved. Since Eq. 16 is based upon simplifying assumptions, it has to be changed to the following form (Brown and Bruhn, 1998).

$$k_{ij} = \lambda A^2 \phi_C \left(\delta_{ij} - n_i n_j\right) \quad \text{.....17}$$

where the factor λ varies from zero to 1/12 depending upon the crack porosity. It is the determination of this parameter that makes any correlation of crack porosity to crack permeability. However, if this parameter can be determined, the problem of connecting the seismic response to production data is solved. This issue will discussed in more detail later in the report.

In summary of this section, fracture aperture is a more useful approach to describing the strength of a fracture because it leads to the crack porosity rather than crack density as the controlling factor for seismic anisotropy. Crack porosity is no easier to validate than crack density. However, since both the crack permeability and the seismic response depend upon the crack porosity, there is a natural relationship between the two measurements that can be utilized by combining seismic and production tests. This relationship will be emphasized later in a discussion on correlating seismic data with production tests.

Predicting Saturation Effects Upon Seismic Response From Fractured Reservoirs. This section presents a discussion of the effects of saturation upon fractured reservoirs. Using the modeling concepts described in the previous section, elastic models for dry fractured rocks (referred to here as dry rock models) can be constructed. Once the dry rock properties are known, the classical results of Brown and Korringa (1975) can be used to predict the effects of saturation upon the dry rock model. A brief review is given of Brown and Korringa's results (1975) and a discussion of the implications follows. The results have some important implications for shear waves.

Brown and Korringa (1975) generalized the Gassmann equation and extended it to the anisotropic problem using relationships between partial derivatives. Their results for the anisotropic problem led to the following formula for the effective (*) compliance.

$$S^A_{ijkl} - S^*_{ijkl} = \frac{\left(S^A_{ij} - S^M_{ij}\right)\left(S^A_{kl} - S^M_{kl}\right)}{\left[\left(K_F - K_\phi\right)\phi + \left(K_A - K_M\right)\right]} \quad \text{.....18}$$

The S_{ijkl} with superscript A represent the dry rock or "drained" compliance. The S_{ijkl} with superscript M represent the compliance of the "solid" rock. A discussion of why "solid" is placed inside of quotes will be given below. In order to compute the terms with two indices (subscripts A or M), the corresponding S_{ijkl} with superscript A or M are contracted (reduced from four to two indices) using the following rule.

$$S_{ij}^{M} = S_{ijkl}^{M}\delta_{kl} = S_{ijkk}^{M} \quad \text{.....19a}$$

$$S_{ij}^{A} = S_{ijkl}^{A}\delta_{kl} = S_{ijkk}^{A} \quad \text{.....19b}$$

Finally, the scalar terms represent further contractions to describe simple hydrostatic pressure experiments.

$$K_A = S_{iijj}^{A} \quad \text{.....20a}$$

$$K_M = S_{iijj}^{M} \quad \text{.....20b}$$

$$K_\phi = -\frac{1}{V_\phi}\left(\frac{\partial V_\phi}{\partial p_F}\right)_{\sigma_{ij}^{d}} \approx S_{iijj}^{M} \quad \text{.....20c}$$

The last term is not directly related to the "solid" (M) or the dry rock (A) properties. Instead, the last term is the relative change of the pore volume with respect to a change in pore fluid pressure (keeping the differential stress constant). If the "solid" is homogeneous, this term is expected to be equal to the contraction of the "solid" (M) compliance as indicated. In practice, rocks are inhomogeneous and the accuracy of this approximation should be challenged.

The ϕ in Eq. 17 refers to the connected porosity. Connected porosity transmits pore pressure and is a measure of the portion of porosity through which flow is controlled. If all of the porosity of a rock is connected, then the "solid" compliance represents the compliance of the solid minerals or grains from which the rock is constructed. If some of the porosity is unconnected, then the "solid" (M) compliance is the effective compliance of the mineral grains and the unconnected pore space. In addition, if there filled cracks, they have to be treated as a part of the "solid." This is why the term "solid" is put in quotes.

As outlined above, in order to apply the results of Brown and Korringa (1975) to fluid saturation studies, the dry rock or drained compliance (superscipt A) has to be determined as well as the compliance of the "solid" (effective grain modulus). The drained property of a rock is really frequency dependent and depends upon the fluid present. This topic will be discussed in future reports. For now, we assume that we can treat the drained and dry properties as being equal. The simple crack models described in the first section of the report can be used to model the dry or drained rock compliance. For the "solid" we can make the simplifying assumption that its compliance is equal to that of the mineral grains (ignoring for now any unconnected or filled cracks). For the purposes of the discussion given here, the pore space compliance is assumed equal to the solid compliance. This is equivalent to assuming homogeneity for the "solid." Once the important solid factors, i.e., the dry rock and "solid" rock, for the Brown and Korringa (1975) equation are determined, the remaining factor to be determined is the compressibility of the saturating fluid. Generally the assumption is made that the fluid is a homogeneous mixture with an effective modulus determined by Wood's equation. However, patchy saturation is believed to modify the properties from those predicted using a homogeneous fluid. For the purposes of this

report a homogeneous fluid is assumed. The assumptions and ideas discussed above are used to point to specific predictions regarding the effects of saturation upon fractured reservoirs.

Vertically Aligned Fractures. An examination is made of the saturation effects upon the elastic properties of a fractured reservoir with a tight matrix. The fractures are vertically aligned in one direction. The saturation effects are based upon the assumptions previously discussed. The term "tight" matrix is used to indicate that there is no porosity in the matrix. All of the "connected" porosity is assumed to be fracture porosity. In this case the dry rock (A) compliance can be written in the form.

$$S^{A}_{ijkl} = S^{Background}_{ijkl} + S^{C}_{ijkl} \quad \text{.....21a}$$

$$S^{A}_{ijkl} = S^{M}_{ijkl} + S^{C}_{ijkl} \quad \text{.....21b}$$

where superscript C is the estimated excess compliance due to the fractures and superscript M is assumed here to be the solid mineral from which the matrix is constructed. The compliance with superscript C can be estimated using the results described earlier for fractures. In this way an estimate of the dry rock compliance is obtained.

Eq. 18 equates the effective compliance to the dry rock compliance with a correction term for any fluid present in the connected pores. Substituting Eq. 21 leads to a fluid correction term in the form

$$fluid\_correction\_term = -\frac{\left(S^{C}_{ij}\right)\left(S^{C}_{kl}\right)}{\left[\left(K_F - K_\phi\right)\phi + \left(K_A - K_M\right)\right]} \quad \text{.....22}$$

This is an important result. It predicts that any saturation effects in a fractured reservoir with a tight matrix depend entirely upon the excess compliance due to the fractures.

Now assume that a single set of aligned fractures exists with their normal pointed along the X1 axis. The excess crack compliance for this system can be written in the 6 by 6 Voigt matrix form (e.g., Schoenberg and Sayers, 1995),

$$S^{C} = \begin{bmatrix} Z & 0 & 0 & 0 & 0 & 0 \\ 0 & 0 & 0 & 0 & 0 & 0 \\ 0 & 0 & 0 & 0 & 0 & 0 \\ 0 & 0 & 0 & 0 & 0 & 0 \\ 0 & 0 & 0 & 0 & Z & 0 \\ 0 & 0 & 0 & 0 & 0 & Z \end{bmatrix} \quad \text{.....23}$$

where Z is the specific compliance of the crack system.

The compliance in Eq. 23 therefore controls the effect of saturation upon the propagation through this simple fractured reservoir. A closer look at this expression gives us a clear picture of how saturation affects the tight matrix fractured reservoir being considered here. Because of the way in which the contraction process used in Brown and Korringa's (1975) equation takes place,

the upper left-hand quadrant of the crack compliance controls the effect of saturation upon P-waves. The upper right-hand and/or the lower left-hand quadrants (because of symmetry) control the effect of saturation upon S-waves. This allows certain predictions to be made from the form of the excess crack compliance in Eq. 23.

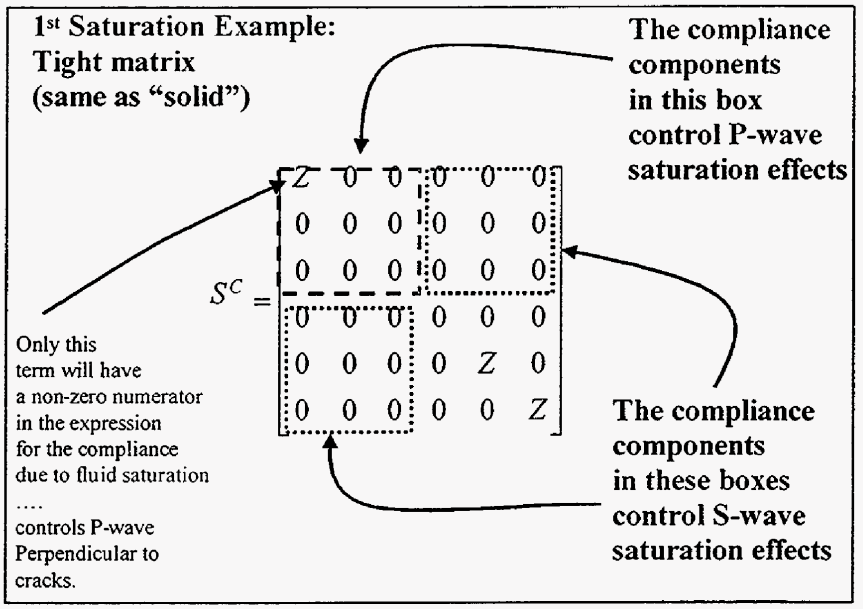

As can be seen in the figure above, only one element of the portion of the compliance governing the effect of saturation upon P-waves (upper left hand quadrant) is non-zero. This element controls the P-wave velocity perpendicular to the cracks. Thus if we are interested in detecting fluid saturation effects with P-waves in a system of vertically aligned cracks, we must have long offset P-waves using surface seismic techniques or we can use crosswell signals in order to attempt to detect the saturation effect perpendicular to the fractures.

Another prediction that can be made from the excess crack compliance concerns the S-waves. Since the quadrants that control the effects of saturation upon S-waves are zero, a classical result is predicted: S-waves are not sensitive to the saturation. In summary of the tight matrix example considered here, two important results have been pointed out. First, P-waves are not sensitive to the saturation of a fractured reservoir with a single set of aligned fractures unless the waves are traveling nearly perpendicular to the fractures. Second, S-waves are not sensitive to the saturation.

Assymmetric Fractures. The nice aspect of Brown and Korringa's (1975) extension of Gassmann's results is that the shear components are predicted, not assumed. In the previous example, the fact that S-waves are not sensitive to saturation was predicted directly. As pointed out, when the upper right and lower left quadrants of the excess crack compliance are zero (for a tight matrix), S-waves are not sensitive to saturation. It is the symmetry (or lack of it) of the dry rock that controls the effect of saturation upon S-waves. The symmetry of a system of vertically aligned fractures is responsible for the vanishing elements that control the effects of saturation upon S-waves.

What type of fracture system will introduce non-zero terms into the quadrants of the excess crack compliance that control the effect of saturation upon S-waves? The answer is simple, one that will break the symmetry of the aligned fracture system described. In other words, a fracture system that introduces non-zero terms into the S-wave quadrants will cause the S-waves to be sensitive to the saturation of a fractured reservoir.

In the picture below, two types of fracture systems are illustrated that can break the symmetry of the vertical system of cracks first discussed. One of the systems of cracks is simply tilted away from the vertical. The other is a rough crack. The rough crack can be modeled as a crack tilted away from the vertical. Both of these fracture models introduce a dry rock anisotropy that makes the S-wave sensitive to the saturation of the reservoir. This is an important result because it means that S-waves can potentially be used in fractured reservoirs to monitor the saturation of the reservoir.

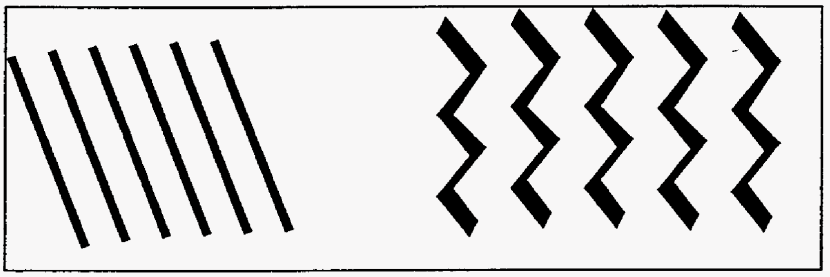

To compliment the above picture for S-waves, Hake et al. (1998) describes an example where an S-wave splitting anomaly was associated with the gas cap for a reservoir. Thus, contrary to the thinking of many people, S-waves can be sensitive to the presence of fluids within fractured reservoirs.

In summary, the problem of saturation for fractured reservoirs depends upon the properties of the dry rock and the "solid." In particular, it is the symmetry of the elements that controls the effect of saturation. Greater symmetry introduces more zeroes into the compliance matrix. An intuitive explanation of why the symmetry plays a role is that when the symmetry is broken, shear stresses applied to the rock act to apply both a normal and a tangential component of force or traction on the surfaces of the cracks. It is the normal component of the traction that is sensitive to the presence of the fluid. When the symmetry is not broken, and the appropriate quadrants in the excess crack compliance are zero, the traction applied to the cracks is primarily tangential and the presence of the fluid is not felt by the S-waves. This means that S-waves can be used to monitor saturation in fractured rocks previously thought to be insensitive to the presence of the saturating fluids and opens up a new avenue of exploration and development work. It means that S-wave "bright spots", i.e., anomalies of increased S-wave splitting, can potentially be used for exploration in the same way that gas bright spots have been used in areas such as the Gulf of Mexico. The advantage here is that the "bright spots" are in older and mature rocks such as those found in many of the major gas plays throughout the onshore in the USA. Specifically, this technology should apply to the midcontinent areas such as Oklahoma.

Seismic Reflection Coefficients Between Anisotropic Media. Now the methods described can be used for predicting the dry rock and saturated elastic properties of fractured reservoirs. In addition, since aperture is the foundation for our models, permeability and the seismic response are linked via the crack porosity. Now we need to evaluate the seismic response to fracture models using the above ideas. One important aspect of the seismic signal is the reflection from the fractured reservoir. In this section the algorithm used for computing the reflection coefficient between two anisotropic media is described.

Much of the theoretical foundation for the algorithm described here can found in the paper by (Rokhlin, 1986). However, the details of the computational procedures used by Rokhlin are not described in his paper. This section emphasizes some of the computational details.

In order to consider the reflection problem for anisotropic media, Rokhlin (1986) emphasizes the following important features of anisotropic wave propagation that distinguish it from isotropic wave propagation.

1) For an arbitrarily selected direction in an anisotropic material, the propagation of three different elastic wave is possible – a quasi-P wave and two quasi-SV waves. For special directions called acoustic axes, the velocities of two quasi-SV waves coincide.
2) The polarization for each of the waves is uniquely determined by the direction of wave propagation. Only for propagation along acoustic axes can the SV wave be arbitrarily polarized as in an isotropic material.
3) Each of the waves has different phase and ray velocities. The ray velocity is greater than or equal to phase velocity and its direction does not coincide with the wave normal.

The Reflection Coefficient Problem. A plane wave is assumed to be incident upon a boundary between two general anisotropic media at a specific angle measured from the normal to the surface of the interface. The components of particle displacement can be expressed as:

$$u_k = AP_k e^{-ik(n\cdot r - Vt)} \quad \text{.....24}$$

where u_k is a component of the displacement vector, A is the amplitude factor of the wave, P_k is the component of polarization vector, $\mathbf{K} = K\mathbf{n} = (\omega/V)\mathbf{n}$ is the vector wave number, $\mathbf{V} = V\mathbf{n}$ is the phase velocity, $\mathbf{n}$ is the unit vector perpendicular to the plane wave front, and $\mathbf{r}$ is the position vector to the point of observation.

A 5-step algorithm is described below for numerically calculating the reflection and transmission coefficients given the elastic properties of the incident and reflecting media. Here these media are assumed to have a general anisotropy.

Step 1: Calculate the phase velocity of the incident wave

The assumed direction of the incident plane wave is used to compute the components n_i (i=1,2,3) of the normal to the wavefront. The Christoffel equation (Rokhlin, 1986) for general anisotropic case can be expressed in the summation-notation form.

$$\det\left(a_{ijkl} n_j n_l - V^2 \delta_{ik}\right) = 0; \mathrm{i, j, k, l} = 1, 2, 3 \quad \text{.....25}$$

where V is the unknown phase velocity of the incidence wave, and the $a_{ijkl} = c_{ijkl}/\rho$ represent the elastic moduli (in tensor form) divided by the density. Thus, for a given wave direction (phase angle), the phase velocity can be obtained numerically from solving the equation (2) which is basically a cubic polynomial in the unkown phase velocity squared (V^2). Some simplifying notation is introduced below so that the method for computing the coefficients of the cubic polynomial are more easily understood.

1. Set $(B_{ik}) = (a_{ijkl}n_jn_l)$, (i, j, k, l = 1, 2, 3), then
2. Expand Eq. 25 into the cubic polynomial form

$$B_{ik} = \sum_{j=1}^{3}\sum_{l=1}^{3} a_{ijkl}n_jn_l \quad \text{.....26}$$

$$C_0 + C_1V^2 + C_2(V^2)^2 + C_3(V^2)^3 = 0 \quad \text{.....27}$$

3. Solve for the phase velocity V of the incident wave from the cubic polyniomial (Eq. 27) using the following coefficients for the polynomial.

$$\begin{aligned} C_0 &= B_{11}B_{22}B_{33} + B_{12}B_{23}B_{31} + B_{13}B_{21}B_{32} - B_{31}B_{13}B_{22} - B_{23}B_{32}B_{11} - B_{21}B_{12}B_{33} \\ C_1 &= B_{31}B_{13} + B_{23}B_{32} + B_{21}B_{12} - B_{11}B_{33} - B_{33}B_{22} - B_{22}B_{11} \\ C_2 &= B_{11} + B_{22} + B_{33} \\ C_3 &= 1 \end{aligned} \quad \text{.....28}$$

Given the phase velocity and normal to the incident wave front, the slowness vector (wave normal divided by the phase velocity) of the incident wave can be computed. The slowness vector of the incident wave is used below to find the slowness vectors of all the reflected and refracted waves. These slowness vectors represent the phase directions. The energy or ray directions have to be computed using methods to be described later.

Step 2: Calculate the 3 reflected and 3 transmitted slowness vectors

Given the incident slowness vector, the slowness vectors of the reflected and transmitted waves have to be determined. By requiring that all waves be in phase at the reflecting interface, a form of Snell's law can be obtained that requires that the component of the slowness along the interface be the same for all waves. Since the incident wave slowness is known, the component of the incident wave slowness is therefore equal to the component of all other waves reflected and refracted from the surface.

The assumption is made here that the reflecting interface is in the x1-x2 plane. The normal to the interface is the x3 coordinate. Using this coordinate system, the vector slowness of a wave is described by the components m_1, m_2, m_3. The m_1 and m_2 components of the slowness will be the same for all reflected and transmitted waves (Snell's law). Our only problem is to find the m_3 component of all of the waves. This is accomplished by using the known m1 and m2 components in a modified form of the Christoffel equation.

$$A = \det\left(a_{ijkl} m_j m_l - \delta_{ik}\right) = 0 \quad \text{.....29}$$

A sixth order polynomial has to be solved in this case. The six solutions represent six wave types. When the upper medium elastic properties are used in Eq. 29, only upgoing (reflected) waves are selected from the six possible solutions. When the lower medium elastic properties are used in Eq. 29, only the downgoing (refracted) waves are selected from the possible solutions. The reflected waves in the upper medium are numbered 1-3 while the transmitted waves are numbered 4-6. Both the upgoing and downgoing waves are placed in order of speed. In most cases studied, this will place the P-wave first. So, for example, m^1 will indicate the slowness for the quasi-P wave, m^2 the slowness for the fastest quasi-S wave and m^3 the slowness for the slowest quasi-S wave. In a like manner, m^4 will be the refracted quasi-P wave and the S-waves arranged in decreasing velocity order as for the reflected waves. This simplistic view is used in order to clarify elements of the presentation. The issue of assigning an identity to the waves requires more explanation than can be given in this report.

The third components m_3^i (i = 1,...6) of the slowness vectors are the unknowns in the sixth-order polynomial (another form of the Christoffel equation) that can be obtained from Eq. 29. The process used is to first calculate the coefficients of the sixth order polynomial represented in Eq. 29 and then solve this polynomial using readily available polynomial solving software.

To create the sixth order polynomial, the following steps are proposed.

1. Calculate the coefficients for quadratic polynomials that make up the determinate matrix in Eq. 29. First, note that each element of the matrix whose determinant is being evaluated in Eq. 29 can be written in the form of a polynomial. Using indices for the coefficients of the polynomials, each term in the matrix can be written in the following quadratic form (right hand side of equation).

$$(a_{ijkl}m_jm_l + \delta_{ik}) = (C_{ik}m_3^2 + D_{ik}m_3 + E_{ik}),\ (i, k = 1, 2, 3) \quad \text{.....30}$$

In order to build these polynomials, first calculate the C_{ik}, D_{ik}, and E_{ik} (3X3) matrices (of coefficients). This notation effectively collects the parameters of the different power of m_3. The coefficients are computed using the following relations.

$$C_{ik} = a_{i3k3} \quad \text{.....31a}$$

$$D_{ik} = (a_{i1k3} + a_{i3k1})m_1 + (a_{i2k3} + a_{i3k2})m_2 \quad \text{.....31b}$$

$$E_{ik} = (a_{i1k2} + a_{i2k1})m_1m_2 + a_{i1k1}m_1^2 + a_{i2k2}m_2^2 + \delta_{ik} \quad \text{.....31c}$$

2. Next, expand Eq. 29 which can be written as Eq. 32 after the computation of the quadratic coefficients, C_{ik}, D_{ik}, and E_{ik}.

$$A=\begin{vmatrix} C_{11}m_3^2+D_{11}m_3+E_{11} & C_{12}m_3^2+D_{12}m_3+E_{12} & C_{13}m_3^2+D_{13}m_3+E_{13} \\ C_{21}m_3^2+D_{21}m_3+E_{21} & C_{22}m_3^2+D_{22}m_3+E_{22} & C_{23}m_3^2+D_{23}m_3+E_{23} \\ C_{31}m_3^2+D_{31}m_3+E_{31} & C_{32}m_3^2+D_{32}m_3+E_{32} & C_{33}m_3^2+D_{33}m_3+E_{33} \end{vmatrix}=0 \quad \text{.....32}$$

The expansion of Eq. 32 is algebraically very complicated. To simplify the process of expanding the above determinant, a procedure is used to divide and conquer the expansion. First expand the determinant in the following form:

$$A=A^{(1)}+A^{(2)}+A^{(3)}+A^{(4)}+A^{(5)}+A^{(6)}=0 \quad \text{.....33}$$

where

$$A^{(1)}=\left(C_{11}m_3^2+D_{11}m_3+E_{11}\right)\left(C_{22}m_3^2+D_{22}m_3+E_{22}\right)\left(C_{33}m_3^2+D_{33}m_3+E_{33}\right) \quad \text{.....34a}$$

$$A^{(2)}=\left(C_{12}m_3^2+D_{12}m_3+E_{12}\right)\left(C_{23}m_3^2+D_{23}m_3+E_{23}\right)\left(C_{31}m_3^2+D_{31}m_3+E_{31}\right) \quad \text{.....34b}$$

$$A^{(3)}=\left(C_{31}m_3^2+D_{31}m_3+E_{31}\right)\left(C_{21}m_3^2+D_{21}m_3+E_{21}\right)\left(C_{32}m_3^2+D_{32}m_3+E_{32}\right) \quad \text{.....34c}$$

$$A^{(4)}=\left(-C_{11}m_3^2-D_{11}m_3-E_{11}\right)\left(C_{32}m_3^2+D_{32}m_3+E_{32}\right)\left(C_{23}m_3^2+D_{23}m_3+E_{23}\right) \quad \text{.....34d}$$

$$A^{(5)}=\left(C_{31}m_3^2+D_{31}m_3+E_{31}\right)\left(-C_{22}m_3^2-D_{22}m_3-E_{22}\right)\left(C_{13}m_3^2+D_{13}m_3+E_{13}\right) \quad \text{.....34d}$$

$$A^{(6)}=\left(C_{211}m_3^2+D_{21}m_3+E_{21}\right)\left(C_{12}m_3^2+D_{12}m_3+E_{12}\right)\left(-C_{33}m_3^2-D_{33}m_3-E_{33}\right) \quad \text{.....34e}$$

Notice that each element $A^{(i)}$ (i = 1, 2,..., 6) is a sixth order polynomial. Each can be expanded into a general sixth polynomial form. The notation used is as follows:

$$\begin{aligned} A^{(i)} &=\left(F_{11}m_3^2+F_{12}m_3+F_{13}\right)\left(F_{21}m_3^2+F_{22}m_3+F_{23}\right)\left(F_{31}m_3^2+F_{32}m_3+F_{33}\right) \\ &=G_0^{(i)}+G_1^{(i)}m_3+G_2^{(i)}m_3^2+G_3^{(i)}m_3^3+G_4^{(i)}m_3^4+G_5^{(i)}m_3^5+G_6^{(i)}m_3^6 \end{aligned} \quad \text{.....35}$$

The F_{ij} represent the polynomial coefficients used in Eq. 34 and the G_i are given below:

$$G_0^{(i)}=F_{13}F_{23}F_{33} \quad \text{.....36a}$$

$$G_1^{(i)}=F_{13}F_{23}F_{32}+F_{13}F_{22}F_{33}+F_{12}F_{23}F_{33} \quad \text{.....36b}$$

$$G_2^{(i)}=F_{13}F_{23}F_{31}+F_{13}F_{22}F_{32}+F_{12}F_{23}F_{32}+F_{11}F_{23}F_{33}+F_{13}F_{21}F_{33}+F_{12}F_{22}F_{33} \quad \text{.....36c}$$

$$G_3^{(i)}=F_{13}F_{22}F_{31}+F_{12}F_{23}F_{31}+F_{11}F_{23}F_{32}+F_{13}F_{21}F_{32}+F_{12}F_{22}F_{32}+F_{11}F_{22}F_{33}+F_{12}F_{21}F_{33} \quad \text{.....36d}$$

$$G_4^{(i)} = F_{11}F_{23}F_{31} + F_{13}F_{21}F_{31} + F_{12}F_{22}F_{31} + F_{11}F_{22}F_{32} + F_{12}F_{21}F_{32} + F_{11}F_{21}F_{33} \quad \text{.....36e}$$

$$G_5^{(i)} = F_{11}F_{22}F_{31} + F_{12}F_{21}F_{31} + F_{11}F_{21}F_{32} \quad \text{..... 36f}$$

$$G_6^{(i)} = F_{11}F_{21}F_{31} \quad \text{.....36g}$$

3. Finally, collecting the coefficients for the different powers of m_3 in the $A^{(i)}$'s from Eq. 33, the sixth order equation in m_3 can be expressed as:

$$A = \sum_{i=1}^{6} G_0^{(i)} + \sum_{i=1}^{6} G_1^{(i)} m_3 + \sum_{i=1}^{6} G_2^{(i)} m_3^2 + \sum_{i=1}^{6} G_3^{(i)} m_3^3 + \sum_{i=1}^{6} G_4^{(i)} m_3^4 + \sum_{i=1}^{6} G_5^{(i)} m_3^5 + \sum_{i=1}^{6} G_6^{(i)} m_3^6 = 0 \text{ ..37}$$

which can be solved for the six values of m_3 (vertical component of slowness) from the sixth order polynomial function in Eq. 37. However, only the physical solutions (usually three out of the six) are used. These are the solutions that satisfy the condition of energy flow in the right direction.

The above procedure must be carried out twice, once for the incident medium and the second time for the refracting medium. Assuming an incident wave propagating downward onto an interface, the energy flow for the three reflected slowness vectors should direct into the upper medium (with positive signs). The three transmitted waves should have energy pointed down into the lower medium (with negative signs). At the critical angle the appropriate ray (or energy flow vector) must be parallel to the interface (Henneke, 1972). After the above procedure has been used to compute vector slowness for each of the reflected and transmitted waves, the direction and phase velocity of the individual waves can be determined. Once these are known, the polarization of each of the waves needs to be determined.

Step 3: Calculate the polarization of each wave

In each direction for the reflected and transmitted waves (defined by slowness vector) $\mathbf{n} = \mathbf{m}/|\mathrm{m}|$, three polarization vectors can be evaluated (one quasi-P and two quasi-transverse) corresponding to the three slowness vectors of the different wave modes in that particular direction. This extra work is not necessary for the quasi-P waves since there is seldom a problem with the polarity of quasi-P waves except for certain exceptional types of anisotropy. However, the extra work is desirable for the quasi-S wave polarizations since the polarization of the quasi-P wave can be used as a reference. These ideas will be expanded below.

If a reflected or transmitted slowness vector **m** have been determined, the polarization of that wave mode can be calculated by determining eigenvectors from the following equation (similar to Eq. 29).

$$\left(a_{ijkl} m_j m_l - \delta_{ik}\right) P_k = 0 \quad \text{.....38}$$

where the m_j are the components of a slowness vector, $a_{ijkl} = c_{ijkl}/\rho$ (c_{ijkl}: elastic constant; ρ: density), P_k is the polarization vector corresponding to the input slowness.

The procedure used for calculating a polarization vector is as follows:

1. Compute the eigenvalue matrix.

Set $(H_{ik}) = (a_{ijkl}m_jm_l-\delta_{ik})$, (i, j, k, l = 1, 2, 3), then

2. Compute the polarization component value.

$$H_{ik} = \sum_{j=1}^{3}\sum_{l=1}^{3} a_{ijkl}m_j m_l - \delta_{ik} \quad \text{.....39}$$

Eq. 38 usually has two non-zero eigenvalues. This means that it has two non-linear equations that can be used for calculating polarization components. The third equation comes from the normalization of the polarization: $\Sigma P_k^2 = 1$. Suppose the *i*th and *j*th (i, j $\subset$ [1, 2, 3]; i $\neq$ j) equations of Eq. 38 are non-linear (in the sense of vectors), then the equations chosen for computing the polarization vector are as follows.

$$H_{i1}P_1 + H_{i2}P_2 + H_{i3}P = 0 \quad \text{.....40a}$$

$$H_{i1}P_1 + H_{i2}P_2 + H_{i3}P = 0 \quad \text{.....40b}$$

$$P_1^2 + P_2^2 + P_3^2 = 1 \quad \text{.....40c}$$

The absolute value of the polarization components can be solved explicitly.

$$P_1 = \frac{1}{\sqrt{1 + A_1^2 + A_2^2}} \quad \text{.....41a}$$

$$P_2 = \frac{A_2}{\sqrt{1 + A_1^2 + A_2^2}} \quad \text{.....41b}$$

$$P_3 = \frac{A_1}{\sqrt{1 + A_1^2 + A_2^2}} \quad \text{.....41c}$$

where

$$A_1 = \frac{H_{j1}H_{i2} - H_{i1}H_{j2}}{H_{i3}H_{j2} - H_{j3}H_{i2}} \quad \text{.....42a}$$

$$A_2 = \frac{H_{j1}H_{i3} - H_{i1}H_{j3}}{H_{i3}H_{j2} - H_{j3}H_{i2}} \quad \text{.....42b}$$

The selection of the proper equations in Eq. 40 requires the equation-selection process described earlier (basically pivoting) to avoid numerical problems. The resulting solution (Eq. 41) can be applied to directly compute the polarization vectors providing all wave phase velocities are different in the wave propagation direction. However, in some cases when the two transverse wave velocities coincide, three independent equations cannot be found and the solution can not be used for calculation of the polarization vector. Wave directions with this property are called acoustic axes, and the polarization vector of the quasi-transverse wave may not be uniquely determined. The quasi-S wave polarization in this case may have any direction in the plane perpendicular to the displacement direction of the quasi-P wave.

In this situation, the desired displacement of the quasi-S wave has to satisfy only one condition: it must lie in the plane whose normal coincides with the displacement of the quasi-P wave. A rule was chosen to find the polarization vectors for the two quasi-S waves when this situation developed. The rule is based upon the assumption that the three polarization vectors (one quasi-P and two quasi-S) for a specific direction of propagation must be orthogonal to each other. Using this assumption, the following procedure was used.

1. Find the quasi-P wave polarization $P^{(p)}$ along the direction of quasi-transverse slowness **m** by solving Eq. 40 for the quasi-P wave.

2. Set one quasi-transverse wave polarization $P^{(s1)}$ orthogonal to $P^{(p)}$ (parallel to the XY plane).

$$P_1^{(s1)} = \frac{-P_2^{(p)}}{\sqrt{(P_1^{(p)})^2 + (P_2^{(p)})^2}} \quad \text{.....43a}$$

$$P_2^{(s1)} = \frac{P_1^{(p)}}{\sqrt{(P_1^{(p)})^2 + (P_2^{(p)})^2}} \quad \text{.....43b}$$

$$P_3^{(s1)} = 0 \quad \text{.....43c}$$

3. Find the other quasi-transverse wave polarization $P^{(s2)}$ by letting it be orthogonal to both $P^{(p)}$ and $P^{(s1)}$ (perpendicular to the XY plane).

$$P_1^{(s2)} = \frac{P_2^{(s1)} P_3^{(p)}}{\sqrt{(P_2^{(s1)} P_3^{(p)})^2 + (P_1^{(s1)} P_3^{(p)})^2 + (P_1^{s1} P_2^{(p)} - P_2^{s1} P_1^{(p)})^2}} \quad \text{.....44a}$$

$$P_2^{(s2)} = \frac{-P_1^{(s1)} P_3^{(p)}}{\sqrt{(P_2^{(s1)} P_3^{(p)})^2 + (P_1^{(s1)} P_3^{(p)})^2 + (P_1^{s1} P_2^{(p)} - P_2^{s1} P_1^{(p)})^2}} \quad \text{.....44b}$$

$$P_1^{(s2)} = \frac{P_1^{(s1)} P_2^{(p)} - P_2^{(s1)} P_1^{(p)}}{\sqrt{(P_2^{(s1)} P_3^{(p)})^2 + (P_1^{(s1)} P_3^{(p)})^2 + (P_1^{s1} P_2^{(p)} - P_2^{s1} P_1^{(p)})^2}} \quad \text{.....44c}$$

Step 4: Selecting the sign for the polarization components

The numerical solution of the direction cosines associated with the polarity P_k does not indicate that the numerical solution points in the direction that obeys conventions used in the literature. The correct signs must be selected for defining the polarization direction according to following rules:

1. For the reflected and transmitted quasi-P waves, the positive polarization direction is selected such that the dot product of the **P** (polarization vector) and **m** (slowness vector) is positive.

$$P \cdot m > 0 \quad \text{.....45}$$

2. For the reflected and transmitted quasi-transverse wave, the normal vector **N** to the incidence plane has to be found first. Then, the positive polarization direction is defined such that the dot product of ***P*** and **N** is positive.

$$P \cdot N > 0 \quad \text{.....46a}$$

$$N = m \times n \quad \text{.....46b}$$

where n is the unit vector normal to boundary plane (Z = 0).

In summary, for reflected and transmitted waves, we have to in general compute the polarization of all three wave types in the directions of the reflected waves in order to handle problems with acoustic axes where the quasi-S polarity can be anywhere in a plane.

Step 5: Calculate reflection and transmission coefficients

Assuming an incident wave with unit amplitude, the boundary conditions of continuity of displacement and stress across the interface can be written in the form of six linear algebraic equations for the reflection and transmission coefficients.

$$P_i^0 + \sum_{v=1}^{6} R^v P_i^v = 0; i = 1,2,3 \quad \text{.....47a}$$

$$C_{j3kl}^0 m_k^0 P_i^0 + \sum_{v=1}^{6} R^v C_{j3kl}^v m_k^v P_i^v = 0; i = 1,2,3 \quad \text{.....47b}$$

where P_i are the polarization components and m_i the slowness components. R^v stands for a reflection or a transmission coefficients depending on the integral value of v between 1 – 6, with the meaning: v = 0 – incidence wave; v = 1 – reflected quasi-P wave; v = 2 – reflected quasi-S wave 1; v = 3 – reflected quasi-S wave 2; v = 4 – transmitted quasi-P wave; v = 5 – transmitted quasi-SV wave 1; v = 6 – reflected quasi-S wave 2. C^v_{j3kl} is the elastic constant of incident medium (if v = 0, 1, 2, 3), or reflecting medium (if v = 4, 5, 6).

Following is the detailed procedure to build the six linear equations in matrix form.

Set

$(I_{m0} + I_{mn}R_n) = 0$; (m, n=1,2,…,6) 48

equivalent to Eq. 47, then

$$I_{mn} = P_{nm}; m = 1,2,3; n = 0,1,2,3 \quad \text{.....49a}$$

$$I_{mn} = -P_{nm}; m = 1,2,3; n = 4,5,6 \quad \text{.....49b}$$

$$I_{mn} = \sum_{i=1}^{3}\sum_{k=1}^{3} C^{(i)}_{(m-3)3ki} m_{nk} P_{ni}; m = 4,5,6; n = 0,1,2,3 \quad \text{.....49c}$$

$$I_{mn} = -\sum_{i=1}^{3}\sum_{k=1}^{3} C^{(r)}_{(m-3)3ki} m_{nk} P_{ni}; m = 4,5,6; n = 0,1,2,3 \quad \text{.....49d}$$

The six reflection and transmission coefficients can be obtained from solving the six linear equations (Eq. 48) with every component expressed explicitly in Eq. 49

The last quantity calculated for the reflected and transmitted waves is the energy flux vector. The energy flux **E** is a vector having the direction of maximum energy flow at a point with a magnitude equal to the amount of energy flowing per unit area perpendicular to **E**. The energy flux **E** and can be expressed as:

$$E_i = \sigma_{ij}\dot{u}_j \quad \text{.....50}$$

A FORTRAN90 subroutine has been written to calculate the reflection/transmission coefficients quasi-P wave and quasi-S waves when provided a incident angle (and the wave mode) upon a boundary between two anisotropic media. The energy-flux vector is used for checking to verify conservation of energy for the reflection and transmission coefficients. It is also used to verify critical refraction (horizontal propagation of energy).

In summary, the algorithm described here and the associated software can be used to compute reflection and transmission coefficients between general types of anisotropic media. This will be especially useful in circumstances when the beds containing the fractures are dipping and/or multiple fracture systems are present. AVO methods cannot be accomplished without the benefit of a general reflection coefficient algorithm such as that described in this report.

AVO Studies of Two Simple Fracture Models. Now the methods described can be used for predicting the dry rock and saturated elastic properties of fractured reservoirs. In addition, since aperture is the foundation for our models, permeability and the seismic response are linked via the crack porosity. Now we need to evaluate the seismic response to fracture models using the proposed ideas. One important aspect of the seismic signal is the reflection from the fractured reservoir. In this section the algorithm used for computing the reflection coefficient between two anisotropic media is described.

A review is given on studies of simple fracture systems in order to investigate the

complexity introduced by multiple fracture systems. One of the problems facing modern seismic exploration is the use of P-wave AVO analysis for characterizing fractured reservoirs. Cores and well logs offer methods of describing fractures but these approaches often suffer from scale effects. The seismic method offers the best approach to characterizing the reservoir at approximately the same scale as that required for predicting reservoir properties.

Since the elastic (seismic) problem is our only concern here, the popular concept of fracture density is used in the model as the controlling factor for the fracture compliance. In addition, the assumption will be used that the excess compliance due to different crack sets can be added.

The emphasis then is an examination of the azimuthal AVO effects of two fractured models using the general-anisotropic reflection coefficient program developed during this project. Model 1 is designed containing a single vertical fracture set and Model 2 contains two fracture sets with different orientations. The interesting result here is that the single fracture set model presents a stronger azimuthal variation in the AVO. A number of problems are identified with the interpretation of multiple fracture sets.

One useful approach in the geophysical literature for describing crack models is via the use of crack or fracture "sets" (e.g., Schoenberg and Sayers, 1995). Each set is a number of parallel cracks that all have the same normal. The results of each crack set (compliance or permeability) is then simply added (neglecting any interaction) as if the results were additive. This approach offers a simple solution that can easily be used in an exploration and development environment.

The excess compliance for cracks can be written in the form (modified from Schoenberg and Sayers, 1995 and Oda, 1983)

$$\bar{S}^{C}_{ijkl} = \frac{Z}{4}\left[\delta_{il} n_k n_j + \delta_{ik} n_l n_j + \delta_{jl} n_k n_i + \delta_{jk} n_l n_i\right] \quad \text{.....51}$$

where Z is the specific crack impedance described earlier. In the models presented here, the specific crack impedance is chosen to give values in agreement with those presented by Hudson (1980, 1981) where Z is expressed as being proportional to the crack density (e). As a reminder, the crack density (e) is the number of cracks per unit volume multiplied times the diameter (D) cubed.

Two models of fractured reservoirs have been set up for a synthetic azimuthal AVO study. The matrix material of the reservoir is assumed to be a carbonate (calcite) with 10% porosity, and the overlying seal layer is shale. Both incident and transmitted layers are assumed isotropic before fracture sets are added to the models. Table 1 lists the petrophysical parameters used as the background information of the models. All these parameters are set within the range of the lithology based upon laboratory measurements and empirical relationships between V_p, V_s and ρ (Castagna, et. al., 1993).

All fracture sets are assumed vertical while the horizontal reflection surfaces are in the (X_1–X_2) plane. Model 1 is assumed to contain one set of fractures with an azimuth of 0° (normals along the direction of X_1 axis pointing east). Model 2 is a set having two sets of fractures at azimuths of 0° and 60°. Figures 1a and 1b show the X_1X_2-plane sketches of Models 1 and 2. The crack density of the fracture set in Model 1 is set equal to 0.1. For the purpose of

comparison study, the total crack density in model 2 is also set as 0.1, with the crack density of each fracture set equal to 0.05. Table 2 lists all the fracture information described above.

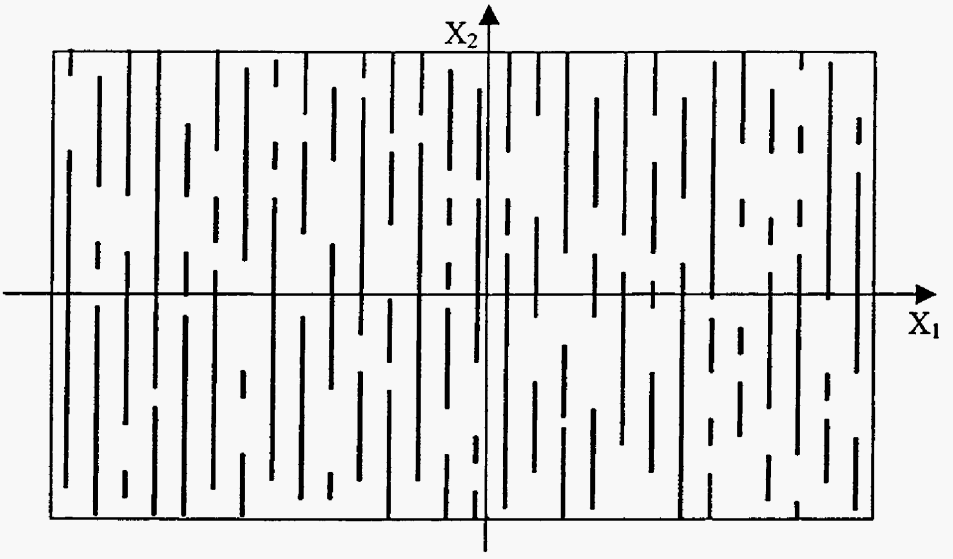

Figure 1a. X_1X_2-plane sketch of single fracture orientation in Model 1.

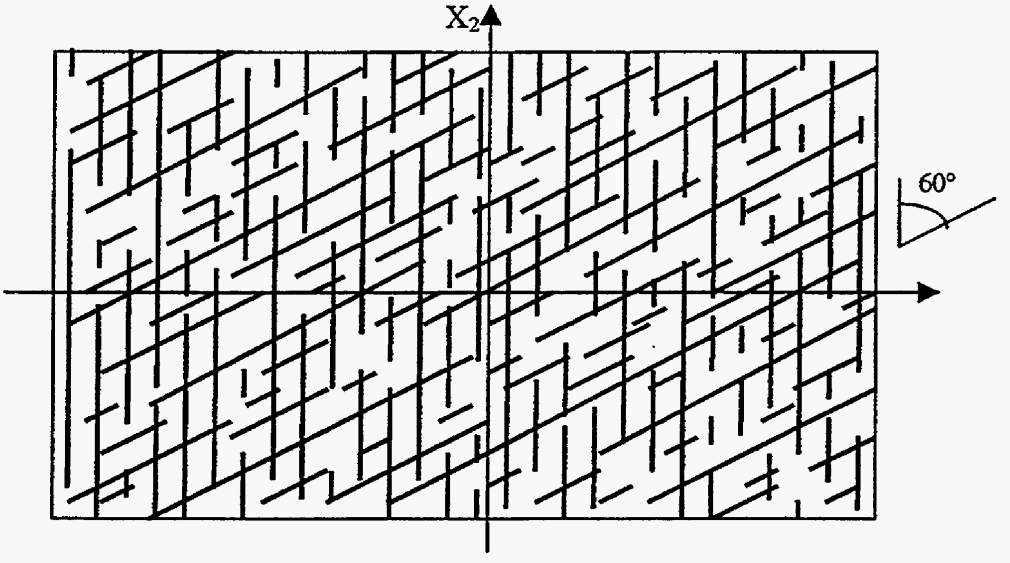

Figure 1b. X_1X_2-plane sketch of model with the two-fracture system used in Model 2

Table 1. Model Matrix Information

Parameter	Reservoir Matrix	Overlying Shale
Vp, m/s	5877	3700
Vs, m/s	3039	1982
Density, g/cc	2.44	2.41
Porosity	10%	

Table 2. Model Fracture Information

Model	Fracture Set	Crack Density	Azimuthal Angle	Dip Angle
1	1	0.10	0	90
2	1	0.05	0	90
2	2	0.05	60	90

For the purposes of this study an incident P-wave is assumed. The three expected reflections are a quasi-P wave (PP), a quasi-in-plane-S wave (PSI), and a quasi-out-plane-S wave (PSO). The incident phase angle for the study is set to range from 0° to 45°. The azimuthal AVO is observed at four different azimuth angles, 0°, 30°, 60°and 90°, respectively. According to Hudson (1980, 1981), one vertical set of the fractures can introduce transverse isotropy with a horizontal symmetry axis (HTI), while multiple sets of fractures cause an arbitrary anisotropy.

Figures 2 and 3 show the exact azimuthal PP reflection from Models 1 and 2, respectively. First of all, comparing these two figures, there are only slight differences in the normal-incidence PP reflection coefficients, showing that the total crack density may be the only key factor related to fractures that influences the zero-offset PP reflections.

Secondly, the azimuthal variations of the PP reflection can be only clearly observed of the models when the incident angle is greater than 25°. Note, however, that Model 1 (with only one fracture set) shows more azimuthal AVO variation than Model 2 (with 2 fracture sets). It is also noticed that, in Figure 3, the azimuth 0° AVO curve is identical to the azimuth 60° AVO curve. At these two azimuths, the incident plane happens to be along the orientation direction of one of the fracture sets. The P-wave sees the same fractured property because the two fracture sets are the same assumed with the model. This can potentially be a useful means of identifying separate fracture sets.

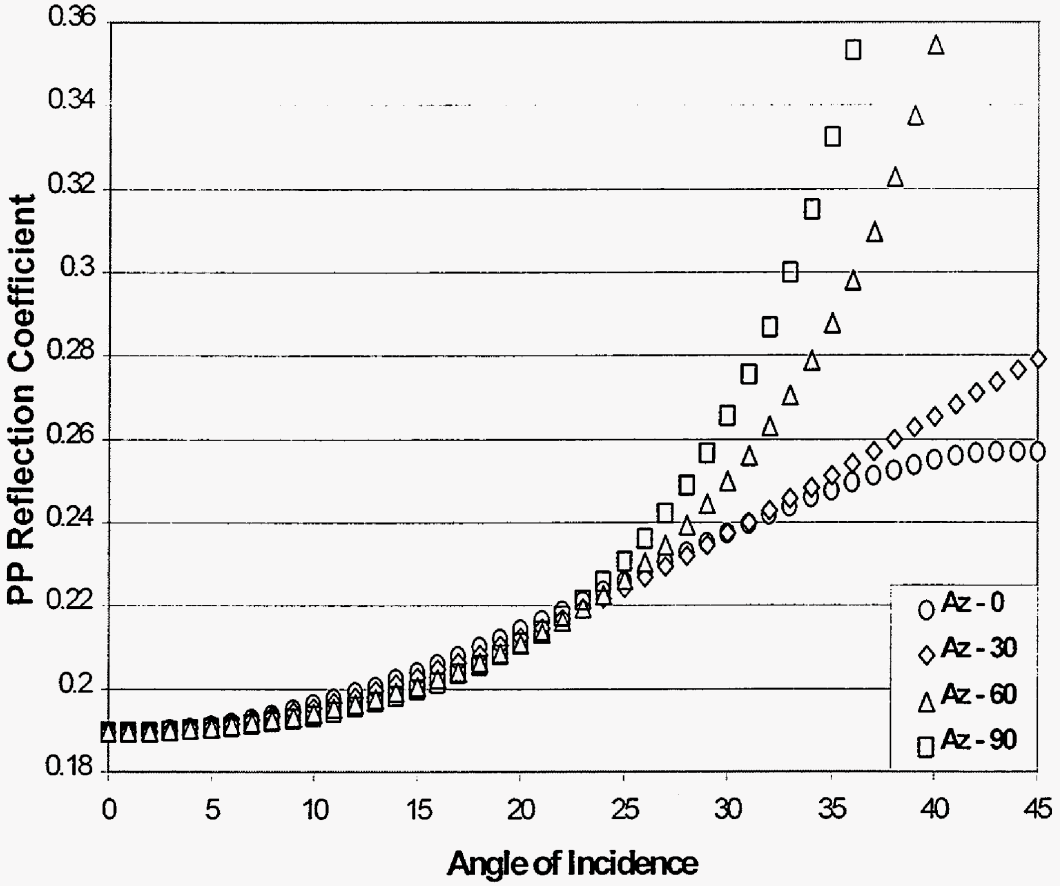

Figure 2. Azimuthal P-wave reflection coefficients for Model 1.

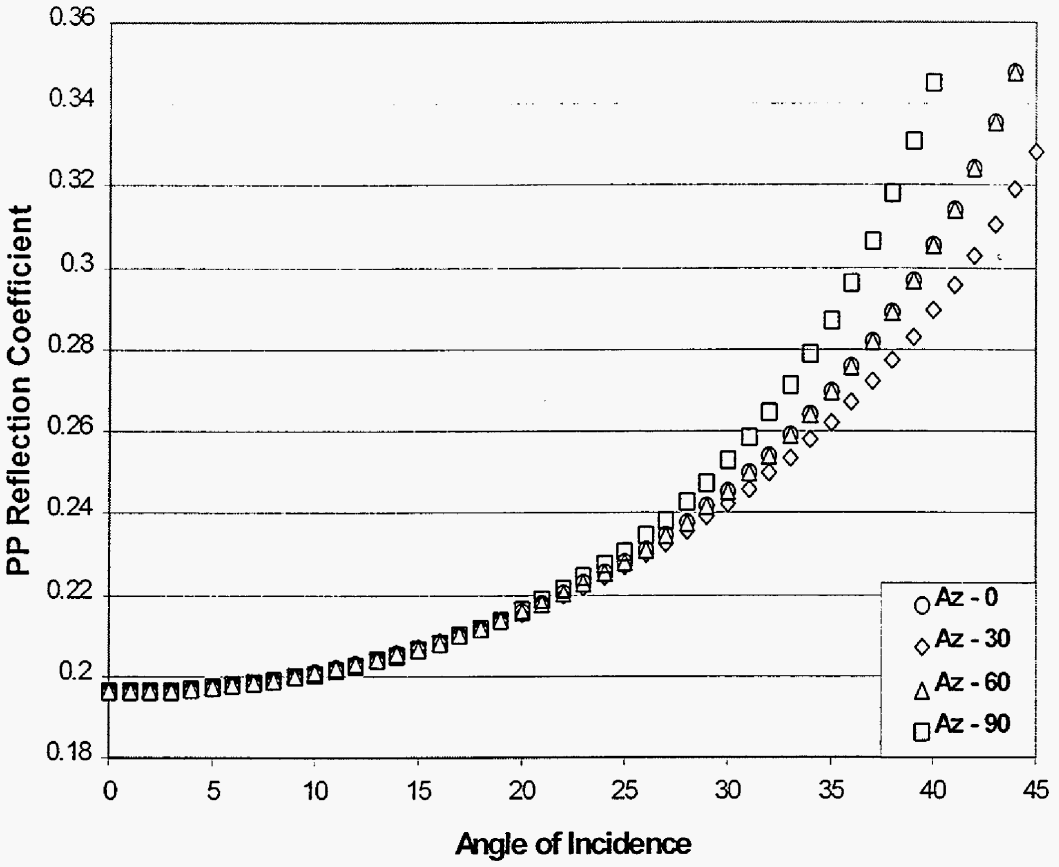

Figure 3. Azimuthal P-wave reflection coefficients for Model 2.

Figures 4 and 5 show the out-of-plane shear reflection coefficients for Models 1 and 2, respectively. Compared with Figure 2 and 3, the azimuthal variation of the converted PS reflections is much more sensitive to fractures than PP reflections. Even for small angles of incidence, Figures 4 and 5 show a more salient azimuthal AVO variation for both Models 1 and 2.

Also, the normal incidence reflection coefficients are always zero for all quasi-S waves because all the fracture sets are vertical. In other words, there is no converted shear wave when the P-wave is normally incident and the axis of symmetry for the anisotropy is vertical.

In Figure 4 for Model 1, notice that the reflected amplitudes for azimuths of 0° and 90° are zero. With only one set of vertical fractures at an azimuth of 0°, the reservoir model can be treated as an HTI medium (Hudson ,1980, 1981). This modeling work shows that shear wave reflection may be useful in finding the orientation of the fracture set under the restrictive condition that only one fracture system exists.

In Figure 5 for Model 2, a zero-reflection curve is also observed. This reflection curve happens at the azimuthal 30°, which is right on the dividing line between the azimuths of 0° and 60° for the two fracture systems present. Notice also that the two reflection curves for the

azimuths of 0° and 60° show up as mirror images of each other corresponding to the curve at an azimuth of 30°.

These observations indicate that the 30° azimuth plane acts as a symmetry plane. However, it is not parallel or perpendicular to any of the fracture sets present. In this multiple fracture model, the plane with an azimuth of 30° can be misinterpreted as an "apparent" or "effective" orientation of a single fracture set.

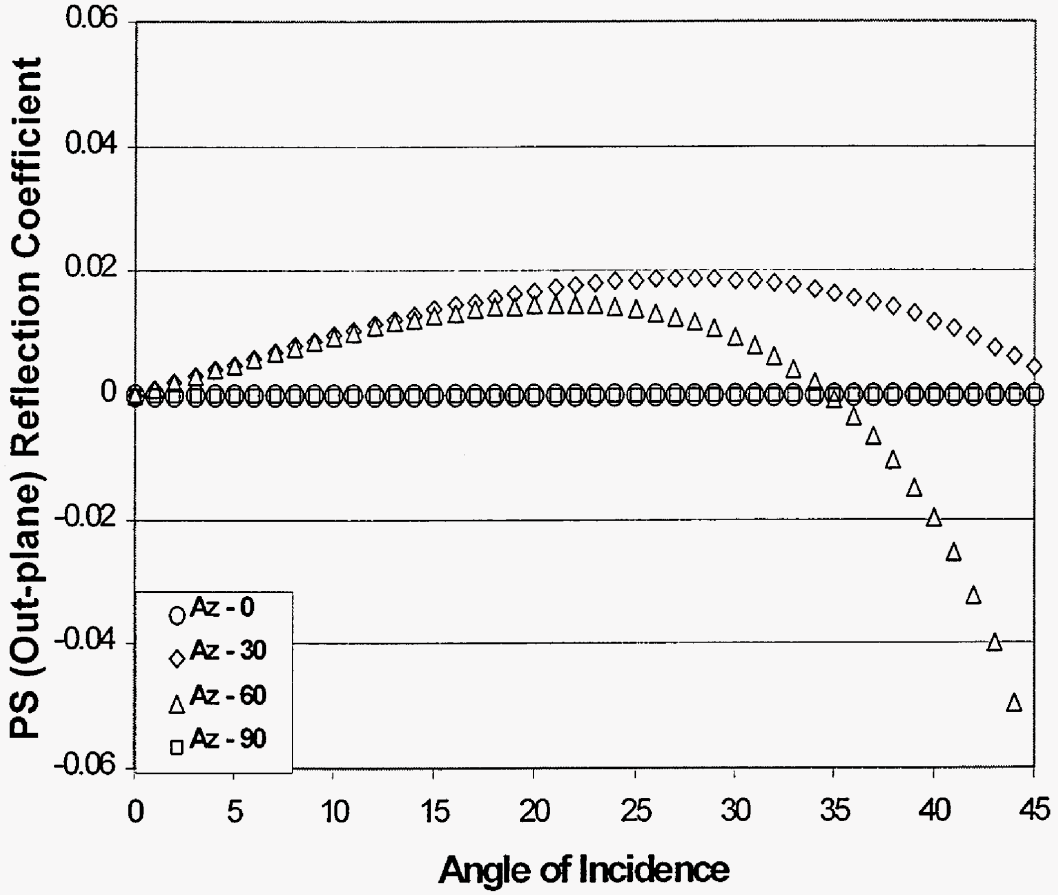

Figure 4. Azimuthal out-of-plane component S-wave reflection coefficients for Model 1.

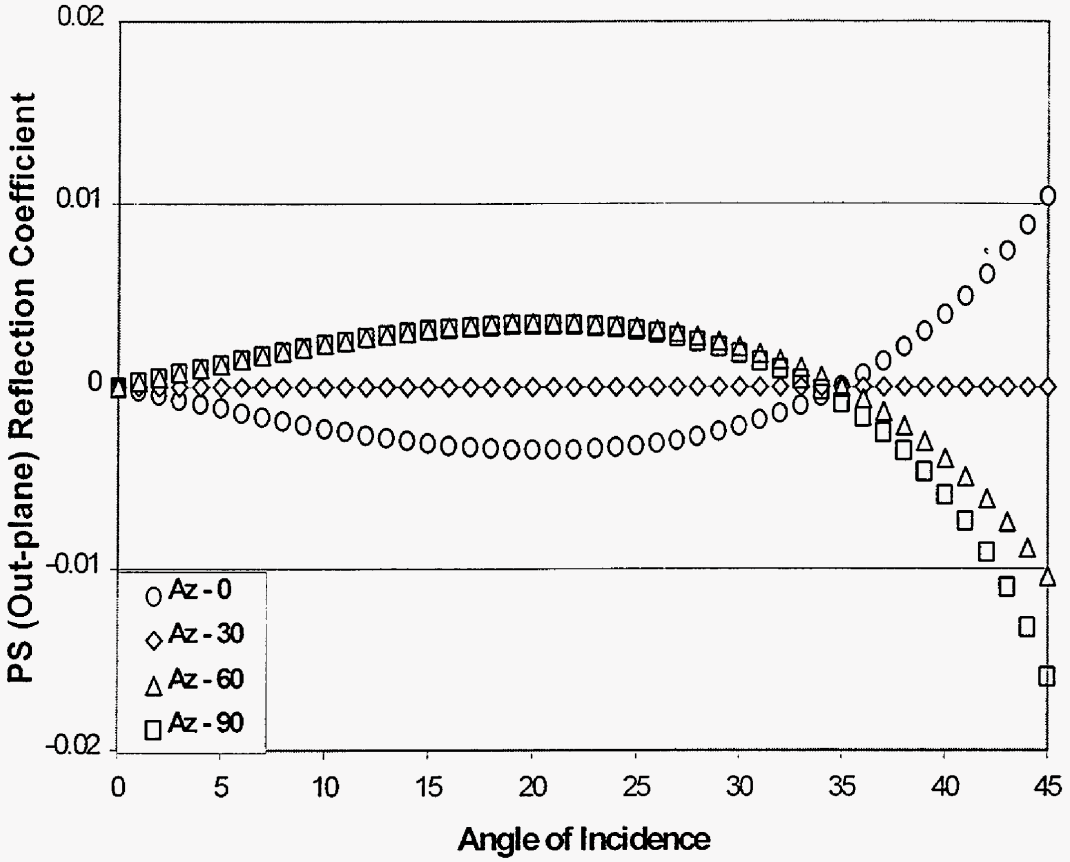

Figure 5. Azimuthal out-of-plane relection coefficients for Model 2.

Figures 6 and 7 show the quasi in-plane shear reflections for Models 1 and 2, respectively. Once again, as with the out-of-plane S-wave, the in-plane S-wave reflection curves show strong azimuthal variations for fracture models under small incidence angle conditions. Even more, the azimuthal AVO are both larger than those of the out-of-plane S-wave curves (compare to Figures 4 and 5). Another observation is that the azimuthal variation of the AVO from the single fracture set model (Model 1) is larger than those of two fracture set model (Model 2).

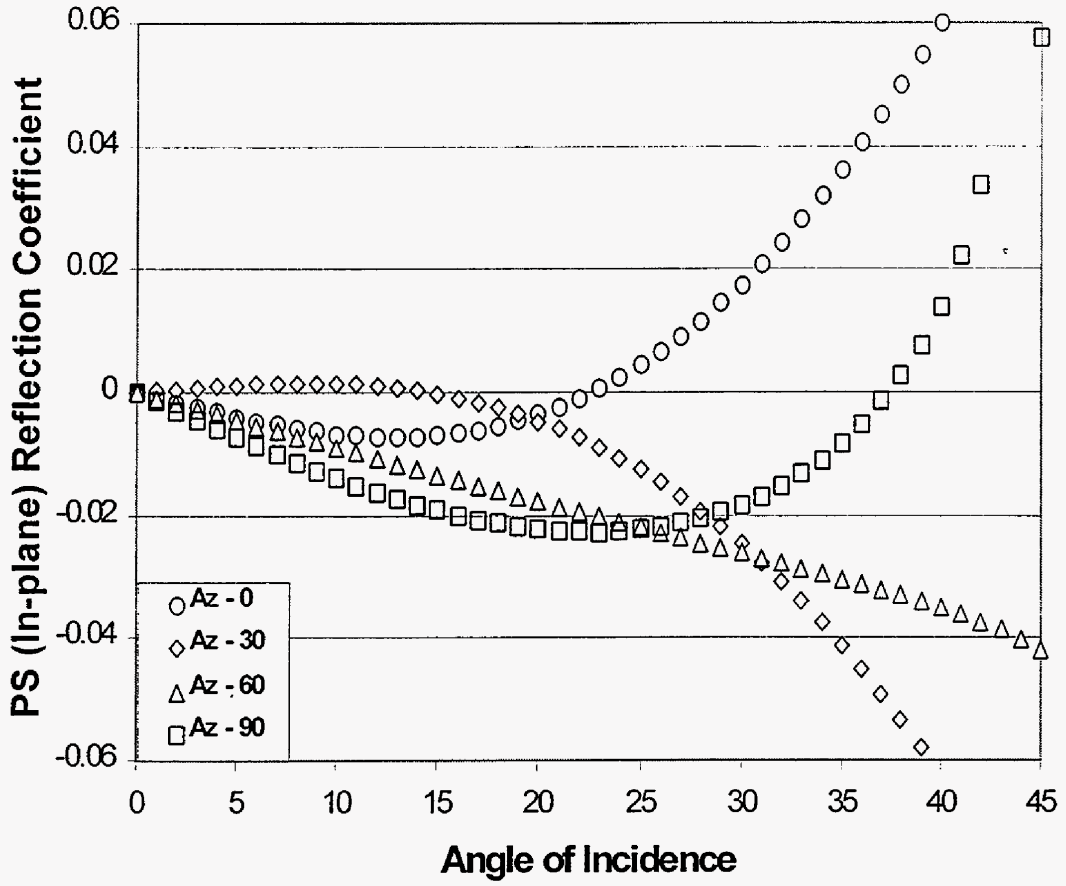

Figure 6. Azimuthal variation of in-plane S-wave reflection coefficients for Model 1.

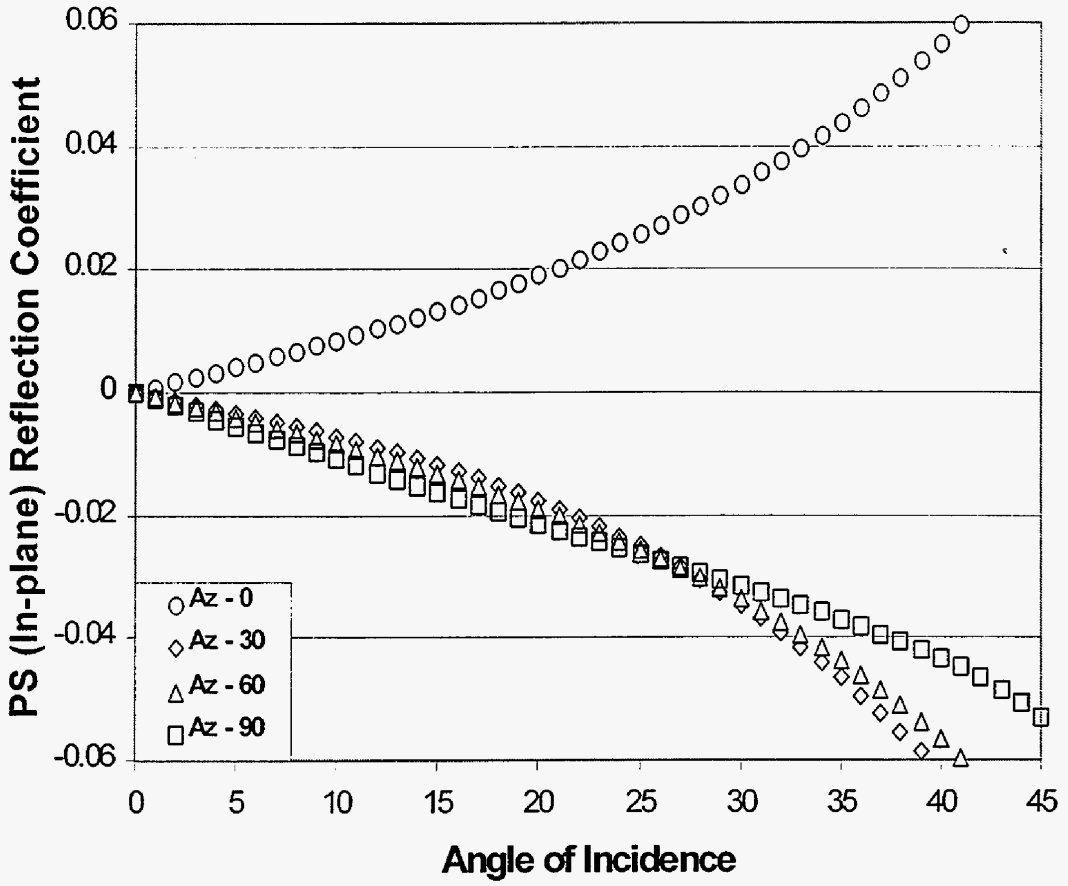

Figure 7. Azimuthal variation of in-plane S-wave reflection coefficients for Model 2.

The azimuthal variation of the converted PS reflections is more sensitive to fractures than the PP reflections. The studies presented here indicate that under small incident angle conditions, S-wave reflection curves still show a distinct azimuthal AVO. However, the azimuthal variations of the PP reflection due to fractures can only be clearly observed when incidence angles are large (>25° in this synthetic study). This means that converted S waves are clearly the exploratory tool of choice if all other factors are equal.

It is also found that when comparing two models with the same total crack density the model containing a single fracture set presents the largest variation on azimuthal AVO. Multiple fracture sets tends to weaken the azimuthal anisotropic effects. With large offset data, the large azimuthal variation in P-wave reflections may indicate the existence of fracture zones. Large azimuthal variations in P-AVO are an indication of a single fracture system. The question remains as to how to interpret this information in a quantitative mode.

The out-plane S-wave azimuthal AVO can be used to find any vertical symmetry planes that may indicate an orientation direction of one fracture set. However, the symmetry plane, under particular situations, may not directly be related to any orientation directions of the fracture sets. Theoretically, in a fractured area, if there is no PS reflection at the normal incident

angle, the fracture sets should be vertical to the reflection boundary. In conclusion, the AVO modeling using the reflection coefficient program has provided a great deal of insight into how to seismically probe fractured reservoirs.

Relating The Seismic Response To Production. In an earlier discussion of an aperture-based approach to fractures, a Z factor, a specific compliance factor, was found that depends upon the crack porosity rather than the more conventional crack density. Although neither crack density nor crack porosity are easy to validate or observe with well control, crack porosity (ϕ_c) has the distinct advantage of being one of the terms that controls both the permeability and the elastic porosity as shown below.

$$k_{ij} = \lambda A^2 \phi_C \left(\delta_{ij} - n_i n_j\right) \quad \text{.....52}$$

$$S^C_{ijkl} = \frac{k_3 \phi_C}{4}(n_j n_k \delta_{il} + n_j n_k \delta_{il} + n_j n_k \delta_{il} + n_j n_k \delta_{il}) \quad \text{.....53}$$

Since production tests and/or production histories provide estimates of permeability, the product of the aperture squared times the crack porosity times an unknown multiplicative factor (λ) can be obtained from such tests ($\lambda A^2 \phi_c$). It is a difficult task to determine either the actual crack porosity or the aperture required for this product using logs or cores. The unknown multiplicative factor (λ) has prevented any successful effort to tie porosity to permeability.

Seismic studies near the same well can produce information on the specific compliance ($k_3 \phi_c$) of the crack system (assuming a single fracture system for the discussion). If a specific model for the crack is used (e.g., Hudson, 1980, 1981), the value of k_3 is known. Thus seismic studies can yield the crack porosity when the value of k_3 is known. However, there are a number of assumptions used when dealing with ideal crack models that may not apply to the problem being studied. This complicates matters even more because both λ and k_3 are unknown. In this case some way of calibrating both of these important constants has to be found.

If the above constants are unknown, some known environment has to be used for calibration. For example, suppose that a well is available with seismic and that well tests have been conducted to determine the permeability. If the well is producing from a "sweet spot" with incredible production, it is probably safe to assume under this circumstance that the λ factor for the permeability is equal to 1/12 (the maximum value assuming excellent connectivity and flow through the fractures). The measured permeability then places a constraint upon the product of the crack porosity and the aperture. If core or other data are available on the fracture apertures, then an estimate of the fracture porosity is obtained from the permeability and aperture estimates.

Once the crack porosity of a site is known, the specific crack impedance determined from the seismic data can be used to determine the elastic constant k_3 from knowledge of Z and ϕ_c (see Eq 15). Once the factor k_3 is known for an area, the seismic response at a well can be used to get an independent estimate of the crack porosity. If the crack porosity is determined at another well via seismic, one has a first step toward predicting the permeability at the well.

The next part of the equation is the estimation of the multiplicative parameter λ that plays a role in the measured permeability. Brown and Bruhn (1998) suggest that λ can be related to the

crack density in a simple functional relationship varying from 0 to 1/12. In terms of the models discussed in this report, the crack density would be replaced by the crack porosity. In this way, the seismic can be used to map permeability throughout the field. However, if λ depends upon other variables, then additional work will be required. For example, some measures of the anisotropy and/or the lack of it, may have to be used in order to better evaluate the connectivity of the systems of cracks.

In summary, a methodology is now in place for calibrating the seismic response to production tests. The procedure is expected to work best when some experience, e.g., in a trend, is available. In this circumstance, the elastic constant k_3 and even the permeability control function λ may be known. The real challenge to this approach is the development of accurate assement of the value of λ..

Task II. Develop Interwell Descriptors of Fractured Reservoir Systems

Characterization of naturally fractured reservoirs requires the integration of well, geologic, engineering, and seismic data. Some of the data is available on a reservoir scale, such as the seismic data, while other data are available at the macroscale, such as well log data. In this task, it is desired to take localized fracture information and scale it for use in characterizing a naturally fractured reservoir and provide input parameters for reservoir simulation studies. To date, effort has been focused on estimating well-based fracture parameters from well log data.

During previous reporting periods, an algorithm and software to estimate the fracture index from conventional well logs have been developed. In addition, an algorithm for prediction of fracture density/intensity from the simultaneous interpretation of various porosity and acoustic logs has been developed.

Work is currently in progress related to scaling well-based parameters and seismic data to develop interwell descriptors. During the current reporting period, a procedure for using a genetic algorithm for the inversion of O'Connell and Budiansky (1984) self-consistent physical model using well log information has been developed to obtain fracture density and aspect ratio.

This model considers a solid permeated with two classes of porosity: crack like, characterized by a crack density with fluid pressure equal to the applied normal stress on the crack face, and pore like (tubes or spheres) characterized by a volume porosity, with fluid pressure substantially less than the applied hydrostatic stress. Fluid flows between cracks at different orientation and between cracks and pores in response to pressure differences.

The model assumes elliptic cracks and spherical pores in order to estimate the strain of a composite rock. The parameters of this model are:

The *crack density*, defined by:

$$\varepsilon = N * \frac{2}{\pi} \langle \frac{A^2}{P} \rangle \qquad \text{.....54}$$

where N is the number of cracks per unit volume, A is the area in plain-form of the crack, and P is the perimeter of the crack.

The *porosity* of the spherical pores, ϕ.

The *bulk modulus of fluid*, K_f.

The *bulk and shear moduli* of the uncracked non porous *matrix* material, K_o and G_o.

The *frequency*, w.

The *characteristic frequency* for fluid flow between cracks, w_s. This parameter can be estimated as:

$$w_s \approx 4\left(\frac{K}{\eta}\right)\left(\frac{c}{a}\right)^3 \quad \text{.....55}$$

where h is the viscosity of the fluid, and c/a is the aspect (thickness to diameter) ratio of the crack.

The modulus is a function of frequency, w, and is a complex number, the real part representing an effective elastic modulus, and the imaginary part representing anelastic energy dissipation. The complex bulk modulus, K, is obtained using Eq. 56.

$$\frac{K}{K_o} = 1 - \frac{\left(1-\frac{K_f}{K_o}\right)\left(\frac{3}{2}\left(\frac{1-v}{1-2v}\right)\phi + \frac{16}{9}\left(\frac{1-v^2}{1-2v}\right)\frac{\varepsilon}{1+i\Omega}\right)}{\left(1+\frac{K_f}{2K}\left(\frac{1-v}{1-2v}\right)\right)\phi + \left(\frac{16}{9}\left(\frac{1-v^2}{1-2v}\right)\frac{K_f}{K}\frac{\varepsilon}{1+i\Omega}\right)}\phi \quad \text{.....56}$$

with

$$\Omega = \frac{16}{9}\left(\frac{1-v^2}{1-2v}\right)\frac{K_o}{K}\frac{w}{w_s} \quad \text{.....57}$$

The shear modulus G is determined using the following relation.

$$\frac{G}{G_o} = 1 - \frac{15(1-v')}{7-5v'}\phi - \frac{32(1-v')}{45}\left(\frac{1}{1+i\Omega'} + \frac{3}{2-v'}\right)\varepsilon \quad \text{.....58}$$

$$\frac{K'}{K'_o} = 1 - \frac{3}{2'}\left(\frac{1-v'}{1-2v'}\right)\phi - \frac{16}{9}\left(\frac{1-v'^2}{1-2v'}\right)\left(\frac{\varepsilon}{1+i\Omega'}\right) \quad \text{.....59}$$

where v' is a fictitious Poisson ratio that satisfies the following.

$$v' = \frac{3K'-2G}{6K'+2G} \quad \text{.....60}$$

The same expression relates the moduli and Poisson ratio of the porous solid.

$$v = \frac{3K-2G}{6K+2G} \quad \text{.....61}$$

Since w_s can be approximated by Eq. 55, then the ratio w/w_s is given by:

$$\frac{w}{w_s} = \frac{w}{4\left(\frac{K}{\eta}\right)\left(\frac{c}{a}\right)^3} = \frac{Asp}{K} \quad \text{.....62}$$

where:

$$Asp = \frac{w\eta}{4\left(\frac{c}{a}\right)^3} \quad \text{.....63}$$

Then Eq. 57 can be rewritten as:

$$\Omega = \frac{16}{9}\left(\frac{1-v^2}{1-2v}\right)\frac{K_o}{K}\frac{Asp}{K} \quad \text{.....64}$$

And Ω` is also given by:

$$\Omega' = \frac{16}{9}\left(\frac{1-v'^2}{1-2v'}\right)\frac{K_m}{K'}\frac{Asp}{K} \quad \text{.....65}$$

If shear and compressional wave velocities are given, then the real part of the bulk and shear moduli (K_r and G_r) can be directly obtained from the following equations:

$$K_r = \rho_b * (V_p^2 - 4/3\ V_s^2) / 10^6 \quad \text{.....66}$$

$$G_r = \rho_b * (V_s^2) / 10^6 \quad \text{.....67}$$

where ρ_b is in gr/cm^3, V_p and V_s are in m/s; Gr and Kr in GPa.

The inversion of O'Connell and Budiansky self consistent model to obtain crack density, e and aspect ratio (c/a) can be seen as an optimization problem, where the goal is to minimize an objective function. If the real part of the moduli (K_r and G_r) are known, the inversion of the model consists of obtaining the parameters e and (c/a) that will minimize an objective function given by:

$$F = |K_r - K_{rcal}| + |G_r - G_{rcal}| \quad \text{.....68}$$

where K_{rcal} and G_{rcal} are the calculated moduli obtained from O'Connell and Budiansky model.

Since the inverse problem is not straightforward, and the equations involved are very complex, this problem is not suitable to be solved through the conventional gradient optimization methods. Instead, a genetic algorithm approach is implemented and programmed in Fortran.

Genetic algorithms (GAs) are a stochastic global search method that mimics the metaphor of natural biological evolution. GAs operate on a population of potential solutions to a problem by applying the principle of survival of the fittest to produce improved approximations to a solution. At each generation, a new set of approximations is created by the process of selecting solutions according to their level of fitness in the problem domain and combining them together using operators borrowed from natural genetics. This process leads to the evolution of populations of individual solutions that are better suited to their environment than the roots that they were created from, just as in the natural adaptation. This process allows an examination of a large sample space of potential solutions and yield near optimal solutions. The GA is terminated when some preselected criteria is satisifed such as total number of iterations, a specified point in the search space is reached, or mean deviation in the population is achieved. Details of GA methods can be located in several references (examples are Goldberg, 1989; Man et al., 1999).

GA differs substantially from traditional search and optimization methods. The most significant differences are:

1. GAs search a population of solutions in parallel, not sequentially.
2. GAs do not require derivative information or other auxiliary knowledge about the functions involved in the problem.
3. GAs work on encoding of the parameter set rather than the parameter set itself.

The chromosome of the GA was formed by a 6 by 8 bit binary string representing 6 variables (K'r, K'c, Kc, Gc, Asp, ε) each with an eight-bit resolution. One point crossover and uniform mutation were applied with operation rates of 0.75 and 0.01 respectively. The population size of 30 was found to work well. For each evolution cycle 29 new offspring were generated while the best chromosome was kept for the next generation. While the program has been developed, it still requires testing.

Task III. Develop Wellbore Models for Fractured Reservoir Systems

During the last project period, work has focused on developing a horizontal wellbore model to use in the naturally fractured reservoir simulator. After a thorough literature review, it was decided to implement a wellbore system that assumes a horizontal wellbore open to flow along its total length and with a homogenous fluid flowing through it. Flow from both the fractures and matrix is allowed to occur and is considered through productivity indexes that are proportional to the equivalent fracture and matrix permeabilities, respectively. A similar approach has been implemented for the vertical well.

Wellbore hydraulics is taken into account by writing the flow equations in a form similar to the reservoir equations. The diffusivity equation that describes oil phase is given by

$$0.006328\ \frac{\partial}{\partial l}\left[\frac{k_p k_{rop}}{\mu_{op} B_{op}}\frac{\partial p_{wf}}{\partial l}\right] = -\frac{\partial}{\partial t}\left(\phi_p \frac{S_{op}}{B_{op}}\right) + 5.615\ Q_o - \left(q_o + q_{of}\right) \quad \text{.....69}$$

where l denotes the coordinate along the wellbore and p indicates that properties are evaluated at the conditions inside of the horizontal pipe, which in the case of PVT properties indicates they are evaluated at p_{wf}. For water, one has a similar equation

$$0.006328\ \frac{\partial}{\partial l}\left[\frac{k_p k_{rwp}}{\mu_{wp} B_{wp}}\frac{\partial p_{wf}}{\partial l}\right] = -\frac{\partial}{\partial t}\left(\phi_p \frac{S_{wp}}{B_{wp}}\right) + 5.615\ Q_w - \left(q_w + q_{wf}\right) \quad \text{.....70}$$

The following relationship can be written for the gas phase accounting for gas solubility in both the oil and water.

$$0.006328\ \frac{\partial}{\partial l}\left[k_p\left(\frac{k_{rgp}}{\mu_{gp}B_{gp}} + \frac{R_{sop}k_{rop}}{\mu_{op}B_{op}} + \frac{R_{swp}k_{rwp}}{\mu_{wp}B_{wp}}\right)\frac{\partial p_{wf}}{\partial l}\right]$$
$$= -\frac{\partial}{\partial t}\left[\phi_p\left(\frac{S_{gp}}{B_{gp}} + \frac{R_{sop}S_{op}}{B_{op}} + \frac{R_{swp}S_{wp}}{B_{wp}}\right)\right] + Q_g - \left(q_g + q_{gf}\right) \quad \text{.....71}$$

The "effective permeability in the pipe" is calculated from a mechanical energy balance where the kinetic and gravity effects are assumed negligible. After writing the homogenous fluid velocity in the wellbore in a form similar to the Darcy velocity of fluids through a porous media, the following expression is obtained for the effective permeability, k_p.

$$k_p = 9.2931\times 10^{9}\ \phi_p \overline{\mu}\left[\frac{r_w}{\overline{\rho} f}\left|\frac{\partial p_{wf}}{\partial l}\right|^{-1}\right]^{\frac{1}{2}} \quad \text{.....72}$$

On the other hand, the pressure drop within the wellbore can be directly calculated from the mechanical energy balance according to the following equation.

$$\frac{\partial p_{wf}}{\partial l} = -2.8914\times 10^{-14}\frac{f\overline{\rho}\,\overline{v}_p^2}{r_w} \quad \text{.....73}$$

By substituting Eq. 73 into Eq. 72, a more convenient expression for k_p is obtained.

$$k_p = 5.4652\times 10^{15}\ \frac{\phi_p \overline{\mu}\, r_w}{\overline{\rho} f \overline{v}_p} \quad \text{.....74}$$

Several terms are involved in Eq. 74 and are explained in the following. The homogenous fluid properties are obtained as saturation weighted averages according to

$$\rho = \rho_{op} S_{op} + \rho_{wp} S_{wp} + \rho_{gp} S_{gp} \quad \text{.....75}$$

$$\bar{\mu} = \mu_{op} S_{op} + \mu_{wp} S_{wp} + \mu_{gp} S_{gp} \quad \text{.....76}$$

The assumption of homogenous fluid is good as long as density and viscosity of phases can be represented by the average mixture properties.

The "equivalent wellbore porosity" is calculated as the ratio of the wellbore volume to the total grid-block (bulk) volume, V.

$$\phi_p = \frac{\pi r_w^2 \Delta l}{V} \quad \text{.....77}$$

The traditional Fanning friction factor, f, is also required in Eq. 74. For laminar flow ($N_{Re} <$ 2100), the friction factor is a function of the Reynolds number according to the following relation.

$$f = \frac{16}{N_{Re}} \quad \text{.....78}$$

For turbulent flow, the friction factor depends on the roughness of the pipe and the Reynolds number. Among several correlations available in the literature, Aziz et al. recommended the equation proposed by Colebrook

$$\frac{1}{\sqrt{f}} = 4 log\left(\frac{r_w}{e}\right) + 3.48 - 4 log\left(1 + 9.35 \frac{r_w}{e N_{Re} \sqrt{f}}\right) \quad \text{.....79}$$

The actual in-situ velocity, v_p, is calculated by dividing the Darcy velocity by the equivalent wellbore porosity

$$\bar{v}_p = -0.006328 \frac{k_p}{\phi_p \bar{\mu}} \frac{\partial p_{wf}}{\partial l} \quad \text{.....80}$$

The solution of Eq. 74 requires an implicit evaluation. Sharma et al. suggested an explicit evaluation using the average in-situ velocity given by Eq. 80. They pointed out that this is a good approximation since pressure gradients and fluid properties do not significantly change between time steps under pseudo-steady-state wellbore flow conditions.

In Eqs. 69-71, linear relative permeability curves are assumed for homogenous flow according to

$$k_{rop} = S_{op} \quad \text{.....81}$$

$$k_{rgp} = S_{gp} \quad \text{.....82}$$

$$k_{rwp} = S_{wp} \quad \text{.....83}$$

The boundary conditions connect the wellbore model with the reservoir model. The fluid transfer term between the matrix and the wellbore is defined as follows.

$$q_i = \tilde{q}_i V \qquad i = o, w, g \quad \text{.....84}$$

where $\tilde{q}_i$ is the flow rate per unit volume of the phase i used as source/sink term in Eqs. 91-93 and V is the grid-block volume. Similar expression can be written for the fluid transfer between the fractures and the wellbore.

Peaceman's approximation was implemented to calculate flow rates from the matrix into the wellbore. For the oil phase, the rate is from the matrix to the wellbore is calculated by

$$q_o = I\left(\frac{k_{ro}}{\mu_o B_o}\right)\left(p_l - p_{wf}\right) \quad \text{.....85}$$

while the following equation is used to calculate the rate from the fracture to the wellbore.

$$q_{of} = I_f\left(\frac{k_{rof}}{\mu_{of} B_{of}}\right)\left(p_f - p_{wf}\right) \quad \text{.....86}$$

where the well indexes, I, are calculated from

$$I = 0.00708 \frac{k_m \Delta l}{ln\left(\frac{r_o}{r_w}\right) + s} \quad \text{.....87}$$

The radius r_O may be estimated from the Peaceman's formula

$$r_o = 0.28 \frac{\left[\left(\frac{k_z}{k_y}\right)^{1/2} \Delta y^2 + \left(\frac{k_y}{k_z}\right)^{1/2} \Delta z^2\right]^{1/2}}{\left(\frac{k_z}{k_y}\right)^{1/4} + \left(\frac{k_y}{k_z}\right)^{1/4}} \quad \text{.....88}$$

The fracture index, I_f, requires fracture characteristics such the permeability scalar in the grid block and fracture half length to calculate the appropriate value.

$$I_f = 0.00708 \frac{|k_f| \Delta l}{ln\left(\frac{L_f}{r_w}\right) + s_f} \quad \text{.....89}$$

On the other hand, Q_i correspond to the imposed injection/production rates from/into the horizontal well. Finally, an auxiliary equation describing the volumetric balance within the horizontal pipe is required.

$$S_{gp} + S_{op} + S_{wp} = 1 \quad \text{.....90}$$

The previous formulation was coded into the naturally fractured simulator but has not been tested. The testing will be conducted during the next reporting period.

Task IV. Reservoir Simulations Development/Refinement and Studies

During this period, modifications to a generalized naturally fractured reservoir simulator developed by Ohen and Evans (1990) based on work proposed by Evans (1982) continued. The simulator is a three-dimensional, three-phase black oil simulator developed to describe fluid flow in a naturally fractured reservoir. Efforts have concentrated on updating the program and incorporating wellbore models within the program. Additionally, steps continue to move the program from a mainframe to a desktop computing environment. The modeling effort is proceeding in a timely fashion.

One major complication with the work discussed in the last progress report was related to unacceptable material balance errors. This problem has commanded a large portion of the project time during the last six months. However, the problem has been solved and was related to the numerical solution of the mathematical model proposed by Evans. Several solutions were explored with a final solution being the modification of the matrix and fractured media relations.

The resulting relations for flow of oil, water, and gas through the matrix are as follows:

$$0.006328 \nabla\left[\frac{\overline{k}_l k_{ro}}{\mu_o B_o}\left(\Delta p_l - \frac{\rho_o}{144} \Delta D\right)\right] = -\frac{\partial}{\partial t}\left(\phi_l \frac{S_o}{B_o}\right) - \tilde{q}_o - \Gamma_o \quad \text{.....91}$$

$$0.006328\,\nabla\left[\frac{\overline{\overline{k_l}}k_{rw}}{\mu_w B_w}\left(\Delta p_l - \Delta P_{cwol} - \frac{\rho_w}{144}\Delta D\right)\right] = -\frac{\partial}{\partial t}\left(\phi_l \frac{S_w}{B_w}\right) - \tilde{q}_w - \Gamma_w \quad \text{.....92}$$

$$0.006328\,\nabla\left[\begin{array}{l}\frac{\overline{\overline{k_l}}k_{rg}}{\mu_g B_g}\left(\Delta p_l + \Delta P_{cgol} - \frac{\rho_g}{144}\Delta D\right) + \\ R_{so}\frac{\overline{\overline{k_l}}k_{ro}}{\mu_o B_o}\left(\Delta p_l - \frac{\rho_o}{144}\Delta D\right) + \\ R_{sw}\frac{\overline{\overline{k_l}}k_{rw}}{\mu_w B_w}\left(\Delta p_l - \Delta P_{cwol} - \frac{\rho_w}{144}\Delta D\right)\end{array}\right]$$

$$= -\frac{\partial}{\partial t}\left[\phi_l\left(\frac{S_g}{B_g} + R_{so}\frac{S_o}{B_o} + R_{sw}\frac{S_w}{B_w}\right)\right] - \tilde{q}_g - \Gamma_g \quad \text{.....93}$$

The matrix permeability is a zero-nondiagonal tensor given by

$$\overline{\overline{k_l}} = \begin{bmatrix} k_x & 0 & 0 \\ 0 & k_y & 0 \\ 0 & 0 & k_z \end{bmatrix} \quad \text{.....94}$$

The fluid interaction term that takes into account the mass transfer from the primary rock matrix into the fractures per unit time per unit volume of the medium is described by the following steady-state approximations for oil, water, and gas.

$$\Gamma_o = C\frac{k_{ro}}{\mu_o B_o}\left(p_l - p_f\right) \quad \text{.....95}$$

$$\Gamma_w = C\frac{k_{rw}}{\mu_w B_w}\left(p_l - p_f - P_{cowl} + P_{cowf}\right) \quad \text{.....96}$$

$$\Gamma_o = C\left[\begin{array}{l}\frac{k_{rg}}{\mu_g B_g}\left(p_l - p_f + P_{cgol} - P_{cgof}\right) + \frac{R_{so}k_{ro}}{\mu_o B_o}\left(p_l - p_f\right) \\ + \frac{R_{sw}k_{rw}}{\mu_w B_w}\left(p_l - p_f - P_{cowl} + P_{cowf}\right)\end{array}\right] \quad \text{.....97}$$

In Eqs. 95-97, the fluid transfer constant, C, is given by

$$C = 0.006328\ \frac{k_m \phi_f}{r_H L_f} \qquad \text{.....98}$$

where k_m is an average matrix permeability obtained from Eq. 94.

The fractured system is modeled as an anisotropic media in which fluids flow according to Darcy's law. In the original model proposed by Evans (1982) an additional acceleration term was included in the equations of motion. However, numerical experiments indicate that the acceleration term contributes with a negligible pressure drop along the fracture. The diffusivity equation that describes the flow through the fractures for oil, water, and gas are as follows.

$$0.006328\ \nabla\left[\frac{\overline{\overline{k_f}} k_{rof}}{\mu_{of} B_{of}}\left(\Delta p_f - \frac{\rho_{of}}{144}\Delta D\right)\right] = -\frac{\partial}{\partial t}\left(\phi_f \frac{S_{of}}{B_{of}}\right) - \tilde{q}_{of} + \Gamma_o \qquad \text{.....99}$$

$$0.006328\ \nabla\left[\frac{\overline{\overline{k_f}} k_{rwf}}{\mu_{wf} B_{wf}}\left(\Delta p_f - \Delta P_{cwof} - \frac{\rho_{wf}}{144}\Delta D\right)\right] = -\frac{\partial}{\partial t}\left(\phi_f \frac{S_{wf}}{B_{wf}}\right) - \tilde{q}_{wf} + \Gamma_w \qquad \text{.....100}$$

$$0.006328\ \nabla\left[\begin{array}{l} \frac{\overline{\overline{k_f}} k_{rgf}}{\mu_{gf} B_{gf}}\left(\Delta p_f + \Delta P_{cgof} - \frac{\rho_{gf}}{144}\Delta D\right) + \\ R_{sof}\ \frac{\overline{\overline{k_f}} k_{rof}}{\mu_{of} B_{of}}\left(\Delta p_f - \frac{\rho_{of}}{144}\Delta D\right) + \\ R_{swf}\ \frac{\overline{\overline{k_f}} k_{rwf}}{\mu_{wf} B_{wf}}\left(\Delta p_f - \Delta P_{cwof} - \frac{\rho_{wf}}{144}\Delta D\right) \end{array}\right]$$

$$= -\frac{\partial}{\partial t}\left[\phi_f\left(\frac{S_{gf}}{B_{gf}} + R_{sof}\frac{S_{of}}{B_{of}} + R_{swf}\frac{S_{wf}}{B_{wf}}\right)\right] - \tilde{q}_{gf} + \Gamma_g \qquad \text{.....101}$$

The fracture permeability is modeled as a nondiagonal tensor given by

$$\overline{\overline{k_f}} = \begin{bmatrix} k_{xx} & k_{xy} & k_{xz} \\ k_{yx} & k_{yy} & k_{yz} \\ k_{zx} & k_{zy} & k_{zz} \end{bmatrix} \qquad \text{.....102}$$

Avila *et al.* (2000) showed that Eq. 102 can be written in a more convenient form. They stated that the fracture permeability tensor can be obtained as a product of two independent functions

$$\bar{\bar{k}}_f = |k_f| \left[\bar{\bar{k}}_f \right] \quad \text{.....103}$$

The unit permeability tensor, $\left[\bar{\bar{k}}_f\right]$, is calculated at specific points in the reservoir where the orientation of the fractures are known. After interpolating/extrapolating fracture orientation in the reservoir domain, the permeability tensor is obtained by multiplying the unit permeability tensor by the permeability scalar, $|k_f|$. In regions of the reservoir where no fractures are present the model exhibits a numerical instability that is overcome by multiplying the unit permeability by the average matrix permeability, k_m.

Auxiliary equations are required to solve this system of equations include the requirement that the saturations in the matrix and the fractures must equal one.

$$S_g + S_o + S_w = 1 \quad \text{.....104}$$

$$S_{gf} + S_{of} + S_{wf} = 1 \quad \text{.....105}$$

In addition, independent capillary pressure relationships for the matrix and the fractures are required as functions of saturation.

$$P_{cowl} = p_l - p_w = f(S_w) \quad \text{.....106}$$

$$P_{cgol} = p_g - p_l = f(S_g) \quad \text{.....107}$$

$$P_{cowf} = p_f - p_{wf} = f(S_{wf}) \quad \text{.....108}$$

$$P_{cgof} = p_{gf} - p_f = f(S_{gf}) \quad \text{.....109}$$

In the general case, the reservoir is modeled as a rectangular parallelepiped with an external no-flow boundary but a constant potential boundary can be easily implemented. The inner boundary condition is either constant rate or pressure as described in the formulation of the wellbore system. The previous partial differential equations were solved using a finite difference formulation and IMPES solution scheme.

After making these changes, the material balance errors disappeared and reservoir simulator capabilities were enhanced. The naturally fractured simulator now has the following characteristics.

1. Numerical simulation of oil and/or gas recovery by fluid expansion, displacement, gravity drainage, and imbibition mechanisms.
2. Rectangular grid-blocks with variable dimensions.
3. Zero transmissibility option (inactive grid blocks).
4. Simulation of tilted reservoirs by specifying the elevations to top of grid-blocks.
5. Porosity and permeability distributions for matrix and fracture systems. For fracture permeability, the model requires a diagonal tensor.
6. Different relative permeability and capillary pressure tables for matrix and fracture systems.
7. Pore matrix and fracture compressibility table.
8. Oil-water-gas PVT tables for reservoir fluids.
9. Bubble point pressure tracking scheme.
10. Pressure and saturation initialization for both porous media.
11. Automatic time-step control.
12. Option for automatic control of LSOR acceleration parameter.
13. Material balance check on solution stability.
14. Vertical and horizontal wells with specification of rate or pressure constraints on well performance.
15. Capabilities to add wells during the time period represented by the simulation.

Task V. Technology Transfer

Technology transfer is an important element of this research project. During reporting periods, informal monthly meetings have been held to share information between the researchers and other interested parties in engineering, geology, and geophysics. Participants have included students, faculty, and researchers from the University of Oklahoma and industry. In addition, one of the principal investigators has developed a fractured reservoir e-mail list server to furnish interested parties regular updates on various topics related to these reservoirs

In July, a paper was be presented before the Society of Exploration Geophysicsts. In addition, several abstracts and papers have been accepted for presentation during 2001 related to the current research project. A one-day seminar was held in December 2000 on naturally fractured reservoirs in Norman. This workshop focused on the progress of the current research. Presenters included the research team. Another one-day seminar will be scheduled for 2001.

The following is a listing of presentations and papers the research team presented during the current reporting period.

Brown, R.L., Wiggins, M.L., and Gupta, A.: "Fracture Roughness: The Key to Relating Seismic Velocities, Seismic Attenuation and Permeability to Reservoir Pressure and Saturation," SEG Annual Meeting and International Exposition, Calgary, August 6-11, 2000.

Conclusion

During the current reporting period, research has continued on characterizing and modeling the behavior of naturally fractured reservoir systems. Work has progressed on

developing techniques for estimating fracture properties from seismic and well log data, developing naturally fractured wellbore models, and modifying a naturally fractured reservoir simulator. The research is currently on schedule as proposed and no obstacles are anticipated for the next six month reporting period.

One aspect of this work involved modifying popular models in terms of crack density to one that depends upon crack porosity. This modification is important because crack porosity is also a used in an estimate of the permeability of a reservoir.simple crack models are used to estimate the "dry rock" properties of a fractured reservoir. The dry rock values can then be used in the results of Brown and Korringa (1998) to predict the effects of saturation upon fractured reservoirs. For vertical cracks aligned in a single direction, this approach predicts that only P-waves are sensitive to the saturation of the reservoir. However, the P-waves are most sensitive to the saturation when traveling perpendicular to the cracks. This means that very long offsets will have to be used. Since long offsets are difficult to record in some areas, this may preclude the use of P-waves for saturation studies. For rough cracks or cracks tilted slightly from the vertical, the S-waves were found to be sensitive to the saturation. Since the S-wave splitting increase is expected for near vertical signals, S-waves show the greatest exploration potential for detecting saturation in reservoirs.

In order to study reflections from fractured reservoirs, software was developed to compute the reflection coefficients. This software has been used to test some of the basic differences between a reservoir with a single fracture system and a reservoir with two fracture systems with different orientations. The results indicate that S-waves hold the key to working out some of the problems related to multiple fracture sets.

A methodology for integrating the seismic and production tests has been developed. The strength of this approach is that no scaling is involved. Here we assume that the seismic scale and the production scale are the same. The goal then is utilize the influence of the crack porosity upon both the permeability and the seismic response. The difficult part will be the characterization of the multiplicative factor that modifies the permeability. This may not be the solution to the problem, but it is definitely a solution that can be used to get answers when other data are sparse.

A genetic algorithm and software program has been developed to obtain fracture density and aspect ratio through the inversion of fractured reservoir rock models using conventional well logs. The software is ready for further testing. Software based on neural networks was develped in prior reporting periods to determine fracture probability from well logs. Fracture probability is an important interwell descriptor of fractures that can be implemented in the definition of permeability tensors. Research suggests a need for logs and interwell measurements of the frequency dependent attenuation of shear and compressional sound waves. Investigation further reveals that cross-well tomography measurements may offer such information. Data from multi-frequency measurements should enhance the information that can be extracted for the description of fractured reservoirs.

Wellbore performance models for vertical and horizontal wells in naturally fractured reservoirs have been devoloped. These models have been incorporated into the naturally fractured reservoir simulator but have not been tested. The development of the reservoir simulator continues in a timely manner. Previous problems related to material balance errors have been corrected by modifying the numerical solution of the flow equations. The simulator is ready for testing.

Research efforts for the next reporting period will concentrate on testing the proposed methods with actual data and formalizing a naturally fractured reservoir characterization methodology. Issues related to upscaling reservoir parameters for reservoir simulation studies and the development of performance models for incorporation into the reservoir simulator will also be addressed. In addition, plans will be made to conduct a one-day technology transfer workshop in mid-2001.

References

Brown, S.R., and Bruhn, R.L., 1998, Fluid permeability of deformable fracture networks: J. of Geophys. Res., 103 (B2), 2489-2500

Brown, R.J.S., and Korringa, J., 1975, On the dependence of the elastic properties of a porous rock on the compressibility of the pore fluid: Geophysics 40, 608-616.

Evans, R.D., 1982, A proposed model for multiphase flow through naturally fractured reservoirs: SPEJ, October, 669-80.

Gassmann, F., 1951, Uber die Elastizitat poroser Medien: Vierteljahrschrift der Naturforschenden Gessellschaft in Zurich, 96, 1-23.

Goldberg, D.E., 1989, *Genetic Algorithms in Search, Optimization and Machine Learning:* Addison Wesley Publishing Company.

Hake, J.H., Gevers, E.C.A., van der Kolk, C.M., and Tichelaar, B .W., 1998, A shear experiment over the Natih field in Oman: pilot seismic and borehole data: Geophysical Prospecting: 46, 617-646.

Henneke II, E.G., 1972, Reflection-refraction of a stress wave at a plane boundary between anisotropic media: J. Acoust. Soc. Am. 51, 210-217.

Horii, H., and Nemat-Nasser, S., 1983, Overall moduli of solids with microcracks: load-induced anisotropy : J. Mech. Phys. Solids, 31 (2), 155-171.

Hudson, J.A., 1980, Overall properties of a cracked solid: Math. Proc. Camb. Phil. Soc. 88, 371-384.

Hudson, J.A., 1981, Wave speeds and attenuation of elastic waves in material containing cracks: Geophys. J.R. Astr. Soc. 64, 133-150.

Man, K.F., Tang, K.S, and Kwong, S., 1999, *Genetic algorithms, concepts and designs*: Springer.

O'Connell, R.J. and Budiansky, B., 1977, Viscoelastic properties of fluid-saturated cracked solids: J. of Geophys. Res. 82(36), 5719-5733.

O'Connell, R.J., 1984, A viscoelastic model of anelasticity of fluid saturated porous rocks: Physics and Chemistry of Porous Media, AIP Conf. Proceedings, 166-175.

Oda, M., 1983, A method for evaluating the effect of crack geometry on the mechanical behavior of cracked rock masses: Mechanics of Materials, 2, 163-171.

Oda, M., Suzuki, K. and Maeshibu, T., 1984, Elastic compliance for rock-like materials with random cracks: Soils and Foundations, 24 (3), 27-40.

Oda, M., 1985, Permeability tensor for discontinuous rock masses: Geotechnique, 35, 483-495.

Oda, M., 1986, An equivalent continuum model for coupled stress and fluid flow analysis in jointed rock masses, Water Resources Research, 22 (13), 1845-1856.

Ohen, H. and Evans, R.D., 1990, Improved simulation of gas/oil drainage and water/oil imbibition in a naturally fractured reservoir: Report to National Institute for Petroleum and Energy Research, Contract 160421.

Rokhlin, S.I., Bolland, T.K., and Adler, L., 1986, Reflection and refraction of elastic waves on a plane interface between two generally anisotropic media: J. Acoust. Soc. Am. 79(4) 906-918.

Schoenberg, M., and Douma, J., 1988, Elastic wave propagation in media with parallel fractures and aligned cracks: Geophysical Prospecting 36, 571-590.

Schoenberg, M. and Sayers, C.M., 1995, Seismic anisotropy of fractured rock: Geophysics 60, 204-211.

Vermilye, J.M., and Scholz, C.H., 1995, Relation between vein length and aperture: Journal of Structural Geology, 17 (3), 423-434.